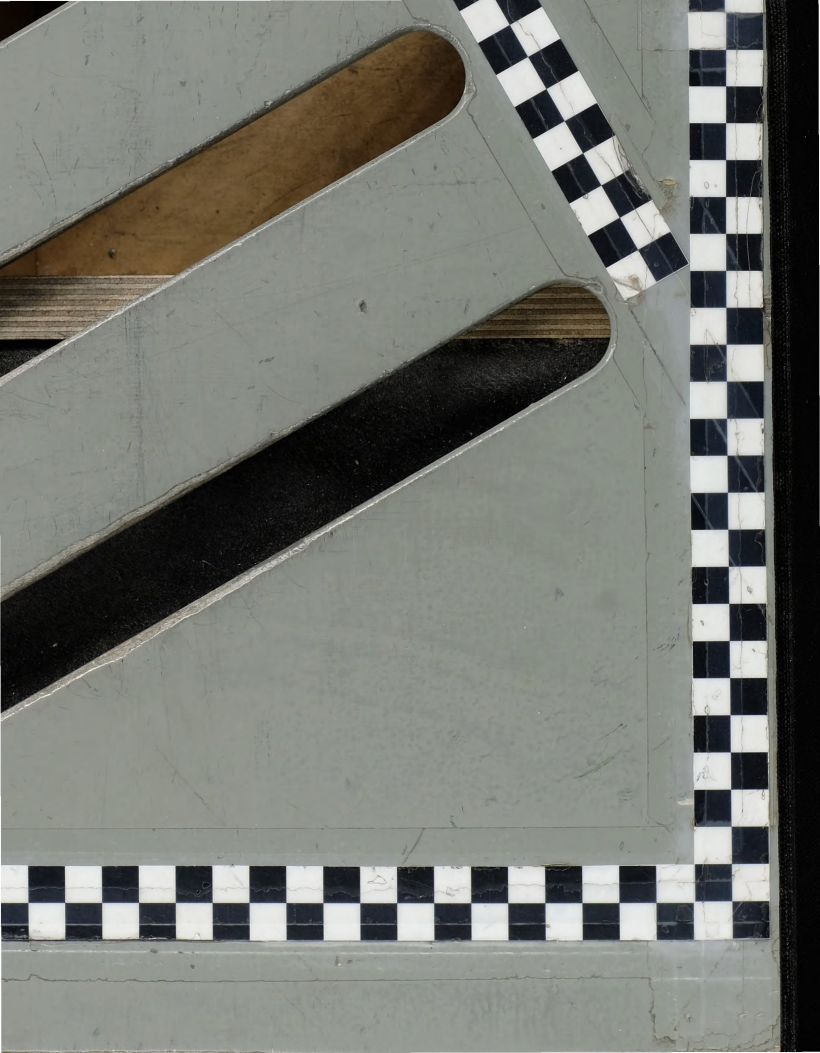

STUDIES OF THE MICROWAVE SPECTRA OF METHYLDIFLUOROPHOSPHINE BORANE, N-METHYLFORMAMIDE, AND N,N-DIMETHYLFORMAMIDE

Thesis for the Degree of Ph. D.
MICHIGAN STATE UNIVERSITY
RIBHI ABDELQADER ELZARO
1973

This is to certify that the

thesis entitled
STUDIES OF THE MICROWAVE SPECTRA OF
METHYLDIFLUOROPHOSPHINE BORANE,
N-METHYLFORMAMIDE, AND
N,N-DIMETHYLFORMAMIDE
presented by

Ribhi Abdelqader Elzaro

has been accepted towards fulfillment
of the requirements for

Ph.D. degree in Chemistry

R. H. Schwendeman
Major professor

Date 2/16/1973

O-7639

ABSTRACT

STUDIES OF THE MICROWAVE SPECTRA OF
METHYLDIFLUOROPHOSPHINE BORANE,
N-METHYLFORMAMIDE, AND
N,N-DIMETHYLFORMAMIDE

By

Ribhi Abdelqader Elzaro

A brief account of the historical development, theoretical treatment, and experimental aspects of microwave rotational spectroscopy is given. Results of investigations of methyldifluorophosphine borane, N-methylformamide, and N,N-dimethylformamide are presented.

The microwave spectra of $CH_3PF_2{}^{11}BH_3$ and $CH_3PF_2{}^{11}BD_3$ have been investigated in the region 18000 to 40000 MHz. The ground state rotational transitions have been assigned for both species. No splittings due to boron quadrupole or internal rotation were observed. The dipole moment was determined to be 3.95 ± 0.05 D. A structural analysis was performed and bond distances and bond angles for a reasonable structure are proposed.

The microwave spectrum of N-methylformamide was studied, and the ground state rotational transitions were assigned for the species in which the methyl group is cis to the carbonyl oxygen. From an analysis of splittings in the ground state rotational transitions the height of the barrier to internal rotation of the methyl group has been

determined to be V_3 = 200 ± 10 cal/mole. The dipole moment is 3.86 ± 0.02 D and the quadrupole coupling constants are χ_{aa} = 2.72 MHz, χ_{bb} = 1.57 MHz, and χ_{cc} = -4.29 MHz. In spite of considerable effort no spectrum could be assigned to a species in which the methyl group is trans to the carbonyl oxygen.

The rotational spectra of N,N-dimethylformamide $(CH_3)_2NCHO$, $(CD_3)(CH_3)NCHO$ (cis) and (trans), and $(CD_3)_2NCDO$ have been studied and ground state rotational transitions have been assigned for each of the isotopic species. The rotational constants are consistent with a planar skeleton for the compound. The barrier to internal rotation for the methyl group cis to the carbonyl oxygen has been determined to be V_3 = 1079 ± 10 cal/mole from a study of the CD_3 species with the CH_3 group cis to the oxygen. The ground state rotational transitions in the CD_3 species with the CH_3 group trans to the oxygen showed no internal rotation splittings which predicts a barrier to internal rotation greater than 2000 cal/mole for the methyl group trans to the carbonyl oxygen. No splittings due to nitrogen quadrupole were resolved for any of the species, and the dipole moment was determined to be 3.85 ± 0.02 D.

STUDIES OF THE MICROWAVE SPECTRA OF METHYLDIFLUOROPHOSPHINE BORANE, N-METHYLFORMAMIDE, AND N,N-DIMETHYLFORMAMIDE

By

Ribhi Abdelqader Elzaro

A THESIS

Submitted to
Michigan State University
in partial fulfillment of the requirements
for the degree of

DOCTOR OF PHILOSOPHY

Department of Chemistry

1973

To My Wife Najla

ACKNOWLEDGMENTS

The author would like to express sincere appreciation to Professor R. H. Schwendeman for his assistance, encouragement, and guidance during the course of this study and preparation of this thesis.

Financial aid in the form of Fellowships from UNESCO and Jordan University are gratefully acknowledged.

TABLE OF CONTENTS

TABLE OF CONTENTS (Continued)

LIST OF TABLES

LIST OF TABLES (Continued)

TABLE

LIST OF TABLES (Continued)

LIST OF FIGURES

I. INTRODUCTION

Gas-phase microwave spectroscopy, as a method for the study of free polar molecules, has been a mature field for more than a decade. In microwave spectroscopy the electomagnetic radiation includes wavelengths ranging from millimeters to a few centimeters -- that is, frequencies of from perhaps 5000 to several hundred thousand megahertz (1-5). The region to higher frequency is often referred to as the submillimeter region; to still higher frequency is the far infrared region where optical rather than electronic techniques become more suitable.

Microwave spectroscopy had its start in 1934 with the historic experiment of Cleeton and Williams (6) on the inversion spectrum of ammonia; no further papers on microwave spectroscopy appeared in the literature until 1946. The concentrated research on microwave radar during World War II provided the necessary instruments and the stimulus for the rapid development of the field which immediately followed the war period. Microwave spectroscopy rapidly proved to be a powerful tool for both physical and chemical research. The method has several unique features which have proved valuable in a variety of chemical problems.

The high specificity of the microwave spectrum makes it well-suited for qualitative analysis. The main requirements are that the substances to be analyzed have sufficient vapor pressure (1-10 μ Hg) and possess a permanent electric dipole moment. Detection sensitivities approaching 1 ppm are possible in the most favorable cases with present instrumentation. A very large number of substances can be detected at a level of one percent and in microgram amounts.

Analyses of microwave spectra provide accurate values for bond distances and angles, dipole moments, bond properties, barriers to internal rotation, nuclear quadrupole coupling constants, nuclear masses, molecular magnetic moments, low lying vibrational frequencies, stereochemical conformations, and energy differences of rotational isomers. New applications are continually being developed, as exemplified by recent studies of ring puckering in four- and five-membered rings (7), polarizability anisotropy (8), magnetic susceptibilities and molecular quadrupole moments (9), and rotational energy transfer (10). These advances have naturally occurred through simultaneous refinements in the experimental, theoretical and computational methods.

It is clear that microwave spectroscopy has provided a considerable quantity of reliable data, often very detailed, on various molecular properties. These data are being built into the structure of chemistry and are also important for testing existing theories and stimulating new theoretical

developments. Although the technique is limited at present to polar molecules (oxygen is an exception) which are not very large and which have some observable vapor pressure, a large number of compounds and probably many new properties and effects remain to be studied. Furthermore, the possibilities of using microwave spectroscopy as an analytical tool have been very little explored (11).

The work reported in this thesis was carried out to study some of the molecular properties and to determine dipole moments, barriers to internal rotation, and structural parameters of the molecules N,N-dimethylformamide, N-methylformamide, and methyldifluorophosphine borane. The first part of this thesis is a discussion of the theoretical and experimental aspects of microwave spectroscopy which are of particular importance in the present investigation. The spectra of the molecules are discussed in Chapters IV, V, and VI.

II. THEORETICAL TREATMENT

2.1 Introduction

It is well known that the energy of an isolated molecule can, to a good approximation, be separated into electronic, vibrational, and rotational parts. In a given electronic and vibrational state most polar molecules in the gas-phase absorb electromagnetic radiation in the microwave region. This absorption increases the rotational energy of the molecules and arises from an interaction of the molecular electric dipole moment with the electric field of the radiation. Rotational energies are quantized and the rotation itself is governed by well-known quantum mechanical formulas (1-5). To a first and very good approximation, a rigid rotating body (12) with three principal mechanical moments of inertia serves as an adequate molecular model for many of the observations. The most important effects of non-rigidity serve only to slightly alter the effective moments of inertia.

Since the rotational behavior of a rigid body is determined by its moments of inertia, which in turn are functions of the geometry and the mass distribution, the microwave spectrum is determined primarily by the geometric structure of the molecule.

2.2 Moments of Inertia

The moments of inertia depend on the positions of the molecular masses with respect to the rotational axes. For a rigid molecule, the moment of inertia about any axis passing through the center of mass is defined by

$$I = \sum_i m_i r_i^2 \qquad (2\text{-}1)$$

where r_i is the normal distance of the i^{th} atom from the axis and m_i is the mass of the i^{th} atom.

If x_i, y_i, z_i are the coordinates of the i^{th} atom and m_i is its mass, then the moments of inertia and the products of inertia are respectively (2,12,13),

$$I_{xx} = \sum_i m_i (y_i^2 + z_i^2) \qquad (2\text{-}2)$$

$$I_{xy} = I_{yx} = -\sum_i m_i x_i y_i \qquad (2\text{-}3)$$

where equations (2-2) and (2-3) are cyclical in x, y, z and the sums are over all the atoms in the molecule.

The moments and products of inertia are the elements of the moment-of-inertia tensor, a second-rank symmetric tensor $\underset{\sim}{I}$.

$$\underset{\sim}{I} = \begin{vmatrix} I_{xx} & I_{xy} & I_{xz} \\ I_{yx} & I_{yy} & I_{yz} \\ I_{zx} & I_{zy} & I_{zz} \end{vmatrix} . \qquad (2\text{-}4)$$

The inertia tensor $\underset{\sim}{I}$ can be diagonalized by means of a similarity transformation which is equivalent to a rotation of the inertial axes. The eigenvalues are called the principal moments of inertia, and the eigen-axis system is called the principal axis system. The three principal moments of inertia are designated as I_a, I_b, I_c. Since the trace of the inertial tensor remains the same under a rotation of axes or by the diagonalization procedure,

$$I_{xx} + I_{yy} + I_{zz} = I_a + I_b + I_c \ . \qquad (2\text{-}5)$$

In case the original coordinate system does not have its origin at the center of mass of the molecule it can be translated to the center of mass. A computer program which calculates the rotational parameters from bond lengths and bond angles has been written by Schwendeman (**14**). The program accepts as input the spherical polar coordinates of each atom, computes the Cartesian coordinates, and subsequently calculates the rotational constants and interatomic distances and angles.

2.3 Rigid Rotor Hamiltonian

In the rigid rotor approximation the energy levels are the eigenvalues of a rotational Hamiltonian which is completely specified by the three principal moments of inertia. The eigenvalue equation is

$$H\Psi = E\Psi \qquad (2\text{-}6)$$

where H is the rotational Hamiltonian operator, Ψ is a

rotational wave function, and E is an eigenvalue.

The rigid rotor Hamiltonian (2) for an asymmetric rotor can be expressed in terms of the rotational constants A, B, and C.

$$H = \frac{4\pi^2}{h} (AP_a^2 + BP_b^2 + CP_c^2) \qquad (2\text{-}7)$$

where $A = \frac{h}{8\pi^2 I_a}$, $B = \frac{h}{8\pi^2 I_b}$, and $C = \frac{h}{8\pi^2 I_c}$ with the usual convention that $A \geq B \geq C$. In Equation (2-7) P_a, P_b, and P_c are the components of the total angular momentum P along the principal axes a, b, and c respectively.

Matrix elements of P_a, P_b, and P_c may be derived from the commutation relationships for angular momentum operators in a rotating Cartesian coordinate system with its origin at the center of mass which are (15),

$$\begin{aligned} [P_x, P_y] &= -i \hbar P_z \\ [P_y, P_z] &= -i \hbar P_x \\ [P_z, P_x] &= -i \hbar P_y \quad . \end{aligned} \qquad (2\text{-}8)$$

A solution of these equations is

$$\begin{aligned} \langle J,K|P_y|J,K+1\rangle &= -i\langle J,K|P_x|J,K+1\rangle \\ &= \left(\frac{\hbar}{2}\right)[J(J+1) - K(K+1)]^{1/2} \\ \langle J,K|P_z|J,K\rangle &= \hbar K \end{aligned} \qquad (2\text{-}9)$$

where J is a positive integer and $K = J, J-1, \cdots, -J$.

The representation used above is that which diagonalizes P_z and $P^2 = P_x^2 + P_y^2 + P_z^2$, and which corresponds to the wave functions chosen by Van Vleck (16) and others. It follows from (2-9) that the non-zero matrix elements of the squares of the angular momentum, which appear in (2-7), are

$$\langle J,K|P_y^2|J,K\rangle = \langle J,K|P_x^2|J,K\rangle = (\frac{\hbar^2}{2})[J(J+1) - K^2]$$

$$\langle J,K|P_y^2|J,K+2\rangle = -\langle J,K|P_x^2|J,K+2\rangle$$

$$= (\frac{\hbar^2}{4})[\{J(J+1) - K(K+1)\}$$

$$X\{J(J+1)-(K+1)(K+2)\}]^{1/2} \quad (2\text{-}10)$$

$$\langle J,K|P_z^2|J,K\rangle = \hbar^2K^2$$

$$\langle J,K|P^2|J,K\rangle = \hbar^2J(J+1) \quad .$$

The calculation of the energy levels of an asymmetric rotor is facilitated by a change of variables and the introduction of an asymmetry parameter, κ, proposed by Ray (17),

$$\kappa = \frac{2B - A - C}{A - C} \quad . \qquad (2\text{-}11)$$

The range of κ is -1 to $+1$; the limits represent symmetric rotors of the prolate symmetric top $(A > B = C)$ and oblate symmetric top $(A = B > C)$ types respectively.

For a symmetric top the Hamiltonian matrix is diagonal and the energy levels can be expressed by a simple closed formula. For a prolate symmetric top the energy level formula is written as

$$E = hBJ(J+1) + h(A-B)K^2 \quad , \qquad (2\text{-}12)$$

while for an oblate top

$$E = hBJ(J+1) + h(C-B)K^2 \quad . \qquad (2\text{-}13)$$

For an asymmetric rotor J is still a good quantum number, but K is not. A convenient way of labeling the energy levels is by using the pseudoquantum numbers K_{-1}, K_1. Thus an asymmetric rotor level is identified uniquely if we specify J and both K_{-1}, the quantum number with which it connects in the prolate limit, and K_1, the quantum number at the oblate limit.

The energy levels of an asymmetric rotor cannot be expressed by a simple closed formula. In general, a secular equation must be solved to obtain the energy. This is readily done with a high-speed computer. A computer program, EIGVALS, written by Hand and Schwendeman for calculating and fitting the rotational spectrum has been in use at this laboratory for several years. Furthermore, several tables of asymmetric rotor energy levels have been published (1,15). It proves convenient to write the energy levels as

$$E = \frac{1}{2}(A + C)J(J + 1) + \frac{1}{2}(A - C)E(\kappa) \qquad (2\text{-}14)$$

where $E(\kappa)$ is a reduced (dimensionless) energy expressed in terms of the asymmetry parameter κ. The chief value of using κ is apparent from the relation, proved by Ray (17),

$$E_{\tau}^{J}(\kappa) = -E_{-\tau}^{J}(-\kappa) \qquad (2\text{-}15)$$

which gives the energies for positive κ from the energies for negative κ, and $\tau = K_{-1} - K_1$.

The transition selection rules for an asymmetric rotor were given by Dennison (18) in terms of a + - notation, and later by Cross, Hainer, and King (19) in terms of K_{-1} and K_{+1}. Since the energy matrices are diagonal with respect to J, the selection rules for J for the asymmetric rotor are the same as for the symmetric rotor. Thus, $\Delta J = 0$, +1, and -1, corresponding to Q, R, and P branch transitions, respectively. The rules for K_{-1} and K_1 can be obtained very easily by means of group theory (19). They depend upon the orientation of the permanent electric dipole moment with respect to the principal axes. Transitions of the a, b, and c types are said to result from the three possible dipole components μ_a, μ_b, and μ_c, respectively. These selection rules may be described by giving the allowed changes in parity of the K_{-1} and K_1 indices. If we designate a level with K_{-1} even and K_1 odd as an eo level, then the allowed transitions are:

a-type: ee <—> eo and oo <—> oe

b-type: ee <—> oo and eo <—> oe

c-type: ee <—> oe and oo <—> eo .

It is, of course, apparent that asymmetric rotors have richer and more complex spectra than linear molecules and symmetric rotors. The intensity of a rotational transition may, in principle, be evaluated by the application of quantum theory, which shows that the intensity of a g-type transition is proportional to μ_g^2 where μ_g is the

component of the total dipole moment along the molecular fixed g axis (g = a, b, c).

2.4 Stark Effect

When a static homogeneous electric field is applied to a molecule having a permanent electric dipole moment, a torque is exerted on the rotating molecule which perturbs its rotational energy. The extent of perturbation of the rotational energy depends on the orientation of the rotational motion with respect to the field as well as the magnitude of the dipole moment. The orientational energy of the permanent dipole moment is given by (1,2),

$$H_\varepsilon = -\bar{\mu}\cdot\bar{\varepsilon} = -\mu\varepsilon\cos\theta \qquad (2\text{-}16)$$

where $\bar{\mu}$ and $\bar{\varepsilon}$ are the electric dipole moment and electric field vectors, respectively, and θ is the angle between these two vectors. If the electric field is assumed to be along the space-fixed z direction, the angular momentum J can assume $2J+1$ orientations with respect to z, corresponding to integral values of M_J from $-J$ to $+J$.

The above perturbation term H_ε can be added to the rigid rotor Hamiltonian, and the resulting eigen value problem can be solved by applying conventional perturbation theory. First-order and second-order perturbation theory yield expressions for the energy which vary with the first and second powers of the electric field, respectively.

A first-order Stark effect can be observed for symmetric top molecules, and for the symmetric-top-like energy levels of asymmetric top molecules, both of which have degenerate or near-degenerate rotational energy levels. The first-order energy for a symmetric top is given by,

$$E_J^{(1)} = \langle \Psi_J^{(0)} | H_\varepsilon | \Psi_J^{(0)} \rangle$$

$$= - \frac{\mu \varepsilon KM}{J(J+1)} \quad . \qquad (2\text{-}17)$$

Since $E^{(1)}$ in equation (2-17) depends on the first power of the quantum number M, each energy level for a given J is split into 2J+1 components.

The above first-order Stark effect was derived on the assumption that the dipole moment is independent of the electric field. Actually the field perturbs the rotational motion, giving rise to an additional component of dipole moment proportional to the electric field and the interaction produces a second-order Stark effect. The second-order Stark effect is much smaller than the first-order Stark effect and can be calculated by using second-order perturbation techniques. Golden and Wilson (20) have calculated the Stark effect of rigid asymmetric rotors by second-order perturbation theory.

$$E_i^{(2)} = \sum_{J \neq i} \frac{| \langle \Psi_i^{(0)} | H_\varepsilon | \Psi_J^{(0)} \rangle \langle \Psi_J^{(0)} | H_\varepsilon | \Psi_i^{(0)} \rangle |}{E_i^{(0)} - E_J^{(0)}} \quad . \qquad (2\text{-}18)$$

After evaluation of the perturbation sum, Equation (2-18)

is usually written as,

$$E_i^{(2)} = \sum_g (A_{ig} + M^2 B_{ig})\mu_g^2 \varepsilon^2 \qquad (2\text{-}19)$$

where $g = a, b,$ or $c,$ and A_{ig} and B_{ig} are called "Stark coefficients". Since $E^{(2)}$ depends on M^2, each energy level is split into $J+1$ components; where J is the lower energy level involved in the transition. The selection rules for rotational transitions depend on the orientation of the applied electric field with respect to the microwave electric field. When the two fields are parallel, the selection rules are $\Delta M = 0$, $\Delta J = 0, \pm 1$. Therefore the rotational frequencies in the presence of the field are given by,

$$\nu = \nu_0 + \nu_s \qquad 2\text{-}20$$

where ν_0 is the zero-field frequency and

$$\nu_s = \varepsilon^2 \sum_g (\Delta A_g + M^2 \Delta B_g)\mu_g^2/h \qquad 2\text{-}21$$

Here ΔA_g and ΔB_g are the differences in A_{ig} and B_{ig} for the energy levels involved in the transition. These quantities depend on the rotational constants of the molecule and on the rotational states involved in the transitions. Once the rotational constants (A,B,C) are known and the transitions assigned, the quantities ΔA_g and ΔB_g can be evaluated by means of the **EIGVALS** computer program. Then the plot of ν_M vs ε^2 yields a slope which is a function of the μ_g^2. This means that the frequencies of the

Stark components must be measured as functions of ε^2 to yield the three independent relations necessary to solve for μ_a^2, μ_b^2, and μ_c^2. For some transitions $\Delta\nu_M$ may only depend upon one or two of the μ_g and therefore evaluation of the dipole moment is simplified.

For transitions involving non-degenerate levels the relative intensities of the Stark components are given by,

$$I(\Delta J = 0) \alpha M^2 \qquad (2\text{-}22)$$

$$I(\Delta J = \pm 1) \alpha (J+1)^2 - M^2 \qquad (2\text{-}23)$$

where J is the lower level involved in the transition.

It should be mentioned that the rotational Stark effect has proved to be excellent technique for obtaining molecular dipole moment, and also for assigning rotational transitions of low J which are often characterized by certain Stark patterns.

2.5 Internal Rotation

The separability of the energy of an isolated molecule into electronic, vibrational and rotational parts is not exact, and interactions between the rotation and vibrational motion always occur in higher orders of approximation. The nonrigidity of the molecule produces several effects which can be observed in the microwave region. One important effect which can influence the microwave spectrum is internal rotation (21). Internal rotation or torsional motion occurs when one part of the molecule rotates about a bond

relative to the rest of the molecule. This motion couples with the overall rotation of a molecule and produces certain effects in its rotational spectrum. Each rotational transition exhibits a fine structure, the complexity of which depends on the height of the potential barrier hindering the internal rotation and on the moments of inertia of the rotating groups. When the internal rotation involves a light group such as the methyl group and is hindered by a moderately high potential barrier (1-2 kcal/mole)—as in trans DMF (d_3), for example — a doubling of most of the ground state transitions is observed in the microwave region. The amount of this splitting leads to a very accurate determination of the hindering potential barrier. The potential function for such a motion should be a periodic function of the relative angle α between the two parts of the molecule, and must be N-fold degenerate as α goes through 2π, where N represents the degree of symmetry of the internal rotor. In the case where the internal rotor has three-fold symmetry, as in ($-CH_3$), ($-BH_3$), ($-SiH_3$), and ($-CF_3$) groups $\cdots$ etc., a good approximation of the potential is

$$V(\alpha) = \frac{V_3}{2} (1 - \cos 3\alpha) \ . \qquad (2\text{-}24)$$

A useful model is one in which the internal rotor is a rigid symmetric top which is attached to a symmetric or asymmetric rigid frame. In this case the Hamiltonian may be written as (2,22),

$$H = H_r + F(P - \rho)^2 + V(\alpha) \qquad (2\text{-}25)$$

where H_r is the rigid rotor Hamiltonian and the coefficient of the second term in Equation (2-25) is the inverse of the reduced moment of inertia for internal rotation:

$$F = \hbar^2/2rI_\alpha \ . \qquad (2\text{-}26)$$

The remaining symbols are defined in Table 1. By expanding the second term in Equation (2-25) it is found that the $F\rho^2$ is quadratic in P_g and hence may be absorbed into H_r. The eigenvalue problem associated with the torsional terms,

$$FP^2 + \frac{V_3}{2}(1 - \cos 3\alpha) \qquad (2\text{-}27)$$

is well known. The boundary condition which is invariance under $\alpha \rightarrow \alpha + 2\pi$ is satisfied by two types of periodic Mathieu functions. The first type has period $2\pi/3$ in α and transforms according to the A species of symmetry group C_3; the second type has period 2π and belongs to the E species. Consequently, each torsional level v consists of two sublevels, a nondegenerate level, $v_A(\sigma = 0)$, and a doubly degenerate level, $v_E(\sigma = \pm 1)$. This partial splitting of degeneracy may be considered to be a result of tunneling through the potential barrier. The tunneling does not directly affect the rotational levels, since the Mathieu eigenvalues are independent of rotational quantum numbers. However, the coupling term in Equation (2-25),

Table 1. Notation[a] for treatment of internal rotation.

g	=	x, y, z refers to principal axis of inertia fixed in the framework.
I_g	=	principal moment of intertia of entire molecule.
I_α	=	moment of inertia of internal top about its symmetry axis.
λ_g	=	direction cosine between top axis and the principal axis g.
rI_α	=	reduced moment of inertia for internal rotation, where $r = 1 - \sum_g \lambda_g^2 I_\alpha / I_g$
P_g	=	component of the total angular momentum along the principal axis g.
$\mathcal{P}$	=	total angular momentum of the internal top along its symmetry axis. $\mathcal{P} = \sum_g P_g \lambda_g / I_g$
J,M,K	=	rotational quantum numbers.
v	=	the principal torsional quantum number for the harmonic oscillator limit.
σ	=	an index which gives the symmetry or periodicity of the torsional eigenfunction. For threefold barrier, $\sigma = 0$ for the A species and $\sigma = \pm 1$ for the E species.

[a] taken from reference 22.

$-2F\rho P$, transmits an effect of the tunneling to the rotational spectrum, since the coupling perturbation differs for the A and E sublevels of a given torsional level.

The Hamiltonian given in Equation (2-25) is diagonal in J, M, and σ, but not in K or v. The elements off-diagonal in K arise from the asymmetry of H_r and also from the terms involving P_x, P_y in the operator ρ and ρ^2. The elements off-diagonal in v come from the perturbation term $-2F\rho P$. As in the case of symmetric molecules, the VanVleck transformation is applied to remove the off-diagonal elements in v so that the new energy matrix assumes the diagonal block structure. The transformed Hamiltonian matrix may then be factored into smaller effective rotational matrices, $H_{v\sigma}$, one for each torsional state.

$$H_{v\sigma} = H_r + F \sum_n W_{v\sigma}^{(n)} \rho^{(n)} \quad . \qquad (2\text{-}28)$$

Herschbach (22) has tabulated the barrier-dependent perturbation coefficients $W_{v\sigma}^{(n)}$ for $n \leq 4$ as functions of a dimensionless parameter s, which in turn is related to the barrier height through

$$V_3 = \frac{9}{4} Fs \quad . \qquad (2\text{-}29)$$

In the asymmetric top basis, specified by eigenstates of H_r, only even n terms in $\sum_n W_{v\sigma}^{(n)} \rho^{(n)}$ contribute to diagonal elements, and only odd n terms to the off-diagonal elements of interest for a slightly asymmetric

rotor. In addition, all the perturbation coefficients of odd order (odd n) vanish for A levels.

Since the perturbation coefficients do not depend on the molecular asymmetry, they may be evaluated (22) in the limit of zero asymmetry, in which the molecule consists of two coaxial symmetric tops. Nielsen (23) has shown that, in the limit of zero asymmetry, the coupling between internal and overall rotation can be eliminated from the Hamiltonian by transforming to an "internal axis" system. Koehler and Dennison (24) have shown that the internal energy levels may be expanded in a Fourier cosine series,

$$W_{v\sigma} = \frac{N^2}{4} \sum_{\ell=0}^{\infty} W_\ell \cos \ell (\theta - \theta_0) \qquad (2\text{-}30)$$

where the coefficients W_ℓ are functions of the torsional level v and the barier parameter s. As $s \rightarrow \infty$ the W_ℓ with $\ell > 0$ vanish very rapidly. The perturbation coefficients given in Equation (2-28) can be related to Equation (2-30) as,

$$W_{v\sigma}^{(n)} = \left(\frac{1}{n!}\right)\left(\frac{2\pi}{N}\right)^n \left(\partial^n W_{v\sigma}/\partial\theta^n\right)_{\theta=0} \qquad (2\text{-}31)$$

and thus they can be expressed as linear combinations of the Fourier coefficients of Equation (2-30).

For moderate barrier heights Equation (2-30) converges very rapidly and it is only necessary to retain the first few terms. Therefore by use of Equation (2-31) the various perturbation coefficients $W_{v\sigma}^{(n)}$ may be approximated in

terms of the first few w_ℓ's. The advantage of this method, the so-called "bootstrap" method is a result of the fact that the higher order $W_{v\sigma}^{(n)}$'s may be written as linear combinations of the lower order of w_ℓ's.

In an alternative method originated by Nielsen (23) and Dennison (24), and called the internal axis method or IAM, the axis about which the top executes internal rotation is chosen as one of the coordinate axes. The other two axes are fixed in the framework. In this coordinate system the terms which describe the interaction between the overall and internal rotation are considerably smaller than those which arise in the principal axes method (PAM). Lin and Swalen (21) have demonstrated the connection between the two methods, and have shown that the Hamiltonian functions can be transformed simply from one method to another through a coordinate transformation.

2-6 Planarity in Amines and Amides

Compounds containing an N-C-O linkage characteristic of amides and polypeptides are important not only spectroscopically, but also biologically.

The pyramidal structure of amines has been thoroughly established; valence angles at the nitrogen atom generally fall in the range $102\text{-}112^0$. In the case of amides, however, a variety of evidence suggests that the three bonds from the nitrogen atom are more or less coplanar. Pauling (25) has represented the above bonding system as two resonating

forms, and has suggested also that the H_2N-C group is planar.

In the first microwave investigation (26) of formamide, H_2N-CHO, it was concluded that this molecule is planar, but a more detailed study of the spectrum by Costain and Dowling (27) gave evidence that the equilibrium position of the amino hydrogen atoms is actually about 0.15Å out of the plane defined by the rest of the molecule.

The microwave spectrum of cyanamide (28,29), H_2N-CN, also suggested a nonplanar equilibrium configuration. However, there are some rather subtle points involved in the decision, on spectroscopic grounds, as to whether the equilibrium configuration of a gaseous molecule is exactly planar. The inference of nonplanarity in gaseous amides is based on the following evidence: (a) the observation of satellite lines in the pure-rotational spectrum which appear to come from very low-lying excited vibrational states, much lower than would be expected from consideration of the normal vibrational frequencies of related molecules; (b) indications of rather high anharmonicity in the vibration responsible for these states; and (c) the unusual behavior, in the case of formamide, of the ground-state intertial defect when an amino hydrogen is replaced by deuterium.

A. The Inertia Defect.

In the principal axis system located in a rigid body of infinitesimal thickness, the following relation is well

established,

$$I_c = I_a + I_b \qquad (2\text{-}32)$$

where I_a, I_b are the two inplane moments of inertia and I_c is the out-of-plane moment. This relationship holds only for a rigid planar molecule. Because real molecules are not rigid, this equation does not hold exactly. Therefore the inertia defect (Δ) for a planar molecule is defined in terms of effective moments of inertia as,

$$\Delta = I_c^0 - I_a^0 - I_b^0 \qquad (2\text{-}33)$$

and is a measure of the deviation from rigid planarity. Oka and Morino (30,31) have written the contributions to the inertia defect as a sum of vibrational, centrifugal and electronic terms,

$$\Delta = \Delta_{(vib)} + \Delta_{(cent)} + \Delta_{(elect)} \cdot \qquad (2\text{-}34)$$

They have calculated the contributions of each of these effects for some c_{2v} triatomic molecules. Upon comparison of the calculated and observed values of the inertia defect in the ground vibrational state, the agreement between these values was quite satisfactory.

For non-planar molecules the quasi-inertial defect (Δ') is defined as

$$\Delta' = I_c - I_a - I_b + \Lambda'' \qquad (2\text{-}35)$$

where Δ'' is the calculated contribution from out-of-plane

atoms. If (Δ') is very close to (Δ) for a non-planar molecule, the molecule is presumed to have a planar skeleton.

The calculation of the inertia defect for molecules other than triatomic may be quite formidable, but as pointed out by Nielsen (32) the inertia defect is not principally a function of the anharmonic part of the potential energy, but rather a function only of the geometry and of the quadratic force constants of the molecule.

B. Anharmonic Vibrations

The potential energy in the normal coordinate system is given as,

$$V = V_0 + \frac{1}{2} \sum_i k_i Q_i^2 + \frac{1}{2} \sum\sum\sum_{ijk} a_{ijk} Q_i Q_j Q_k + \cdots \qquad (2\text{-}36)$$

where k_i is the quadratic force constant, which is harmonic in nature and relatively easy to obtain, for small molecules, by infrared spectroscopy. On the other hand, a_{ijk}, the cubic force constant is very difficult to obtain.

It seems highly probable (27,29) that the low-lying excited vibrational states of amides are associated with the out-of-plane bending vibration of the NH_2 group with respect to the molecular framework. If this bending vibration were described by a parabolic potential function with its minimum at the planar configuration of the molecule, a series of evenly-spaced vibrational levels, designated by a quantum number v, would result. If the system is perturbed by adding a small symmetric potential hump centered

about the planar configuration, it is well known that the levels of even v will move up in energy relative to those of odd v. Thus the levels v = 0 and v = 1 approach each other, as do v = 2 and v = 3, and so on; in the limit where the potential hump is very large the successive pairs become degenerate, yielding the so-called inversion degeneracy of a non-planar molecule (33). A pyramidal model for formamide (27) was proved to have two equilibrium configurations separated by a potential barrier. By fitting the experimental data to a Manning (34) double minimum potential, a barrier of 370 ± 50 cm^{-1} hindering the "inversion-wagging" type of motion was determined.

C. Isotopic Substitution

In 1953 Kraitchman (35) formulated the problem of structure determination in terms of the changes in the moments of intertia between isotopically substituted molecules. For a non-planar asymmetric top Kraitchman's formulation can be summarized as follows:

$$c^2 = \langle (\frac{1}{\mu})(P_c' - P_c)[1+(P_a'-P_a)/(P_a-P_c)][1+(P_b'-P_b)/(P_b-P_c)] \rangle \quad (2\text{-}37)$$

where $$\frac{1}{\mu} = [(M + \Delta M)/M\Delta M \quad (2\text{-}38)$$

and $$P_a = \sum_i m_i a_i^2 = \frac{1}{2}[I_c + I_b - I_a]. \quad (2\text{-}39)$$

Here I_a, I_b, I_c are the principal moments of inertia, the P's are the second moments, defined by Equation (2-39), M is the total mass of the "parent" molecule, and ΔM is the

mass change on isotopic substitution. In Equation (2-37) the primed quantities refer to the isotopically substituted molecule and the unprimed quantities to the parent molecule; Equations (2-37) and (2-39) are cyclical in a, b, and c. The quantities a, b, and c are the coordinates of the substituted atom in the principal axis system of the parent molecule. Costain and Dowling (27) have investigated ten isotopic species of formamide by microwave spectroscopy. The inertia defect was found to decrease whenever a heavier isotope was substituted for any atom in the H_2N group, and in fact was negative for four of the species studied. It was concluded that the molecule is non-planar with the H_2N-C group forming a shallow pyramid. The most probable structure of formamide was given, and the double-bond character of the C-O bond and N-C bond was estimated by using an empirical formula proposed by Pauling (25). The double-bond character in formamide turned out to be 86 percent for the C-O bond, and 25 percent for the N-C bond.

Another parameter, the bond order, may be used to characterize the interaction, if a molecular orbital scheme is considered in which the four P_z or π-bond electrons are mobile over the N-C-O linkage. On the basis of a Hückel molecular orbital (HMO), Kumer and Murty (36) have determined the charges on oxygen, carbon, and nitrogen atoms and have determined also the bond orders of C-O and C-N bonds in several primary, secondary, and tertiary amides.

The result showed that the C-O and C-N bond orders in (DMF) are 1.932 and 1.259 respectively.

The electronic structure of amides is characterized by resonance stabilization, due to the delocalization of the carbonyl, π- and nitrogen lone pair electrons, resulting in an increased double-bond character of the C-N bond and a tendency towards a planar structure.

Formamide (27) has been shown by microwave spectroscopy to have a slightly pyramidal conformation about the nitrogen atom in the gas phase while N,N-dimethylformamide is essentially planar (this work).

III. EXPERIMENTAL

3.1 Introduction

Spectroscopy is essentially a determination of energy levels of molecules, atoms, and nuclei. The experimental methods employed to do this consist, fundamentally, of measurements of frequency, because the energy difference between the two levels involved in a transition determines the frequency of radiation which is emitted or absorbed by the particular molecule, atom or nucleus being investigated. The problem of the experimental spectroscopist is thus to measure the frequency of the emitted or absorbed radiation as accurately as possible.

As in other types of absorption spectroscopy, the essential components of a microwave spectrometer or molecular rotational resonance (MRR) spectrometer are the radiation source, absorption cell, and detector. The source is normally a vacuum tube oscillator; reflex klystron oscillators have received the greatest use, with backward wave oscillators (BWO) next in importance. The output of such tubes is highly monochromatic, but the frequency band width is not perfectly sharp because of environmental fluctuations (electrical, mechanical, and thermal). The output frequency of a klystron may be scanned continuously by a combination of

mechanical and electronic control, while in a BWO the frequency control is entirely electronic.

Microwave radiation is normally transmitted through a waveguide. This is a metal pipe, usually of rectangular cross section, whose dimensions are comparable to the wavelength of the radiation. Waveguides of different sizes are required to cover the full microwave spectrum. The absorption cell is usually sealed with mica windows to the ends of a length of waveguide. A hole in the waveguide wall provides a connection to a vacuum manifold, so that the cell can be evacuated and the gas sample introduced.

The most convenient detector for microwave spectroscopy is a crystal diode, which is attached to the end of the absorption cell. The absorption of microwave power at discrete frequencies is very small. To increase sensitivity, Stark modulation and phase-sensitive detection are used. The Stark-modulated signals are demodulated by the broadband crystal detector. The demodulated 33.333 kHz signal is amplified, phase-detected, and displayed on a meter, recorder, or optional oscilloscope.

Microwave measurements used to require considerable experience and judgment on the part of the operator. However, microwave components are now much improved, and complete spectrometer systems have recently become commercially available. It is therefore possible to concentrate on chemical applications of the method without the necessity of becoming familiar with all of the engineering details.

3.2 Stark Modulation

The very low absorption coefficients in the microwave region place severe requirements on the sensitivity of the detection system. Absorptions as small as one part per million are often measured. Such small changes in the transmitted microwave power are difficult to detect directly, but a great improvement can be achieved by using a Stark modulation scheme (37,38). Here the frequency of the molecular absorption line is shifted periodically by applying an alternating electric field to the gas in the absorption cell, the detection system is then tuned to this alternating frequency. The electric field alternation is ordinarily a square wave pattern at a frequency of 5-100 kHz[1]. The MRR spectrometer on which this work was done is a Hewlett-Packard model 8460A spectrometer, which has a 33.333 kHz modulation frequency. A simplified block diagram of the Hewlett-Packard MRR spectrometer is shown in Figure I.

As a result of the phase-sensitive detection the absorption signals during one phase of the Stark field drive the recorder pen in one direction while the absorption signals during the opposite phase drive the pen in the other direction. Thus, if one half of the Stark field is based at zero voltage, the zero-field spectrum and the Stark spectrum are both recorded in opposition to one another.

---

[1] 1 Hz = 1 sec^{-1}; 1 kHz = 10^3 Hz; 1M Hz = 10^6 Hz; 1 GHz = 10^9 Hz.

Figure I. Model 8460A MRR spectrometer block diagram.
(Reproduced with permission of the Hewlett-Packard Company.)

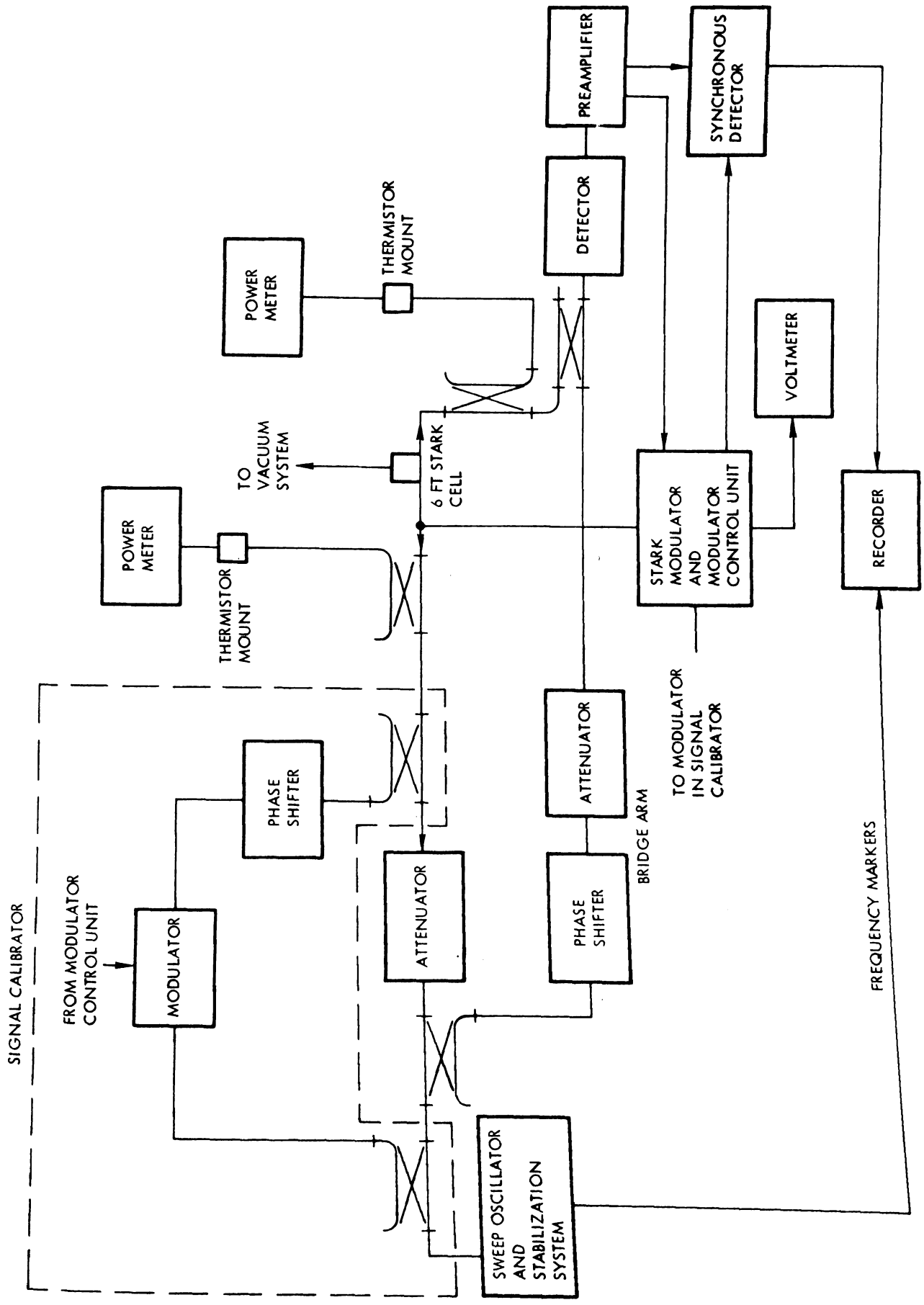
SIGNAL CALIBRATOR
FROM MODULATOR CONTROL UNIT
MODULATOR
PHASE SHIFTER
ATTENUATOR
SWEEP OSCILLATOR AND STABILIZATION SYSTEM
POWER METER
THERMISTOR MOUNT
TO VACUUM SYSTEM
6 FT STARK CELL
POWER METER
THERMISTOR MOUNT
DETECTOR
PREAMPLIFIER
SYNCHRONOUS DETECTOR
VOLTMETER
STARK MODULATOR AND MODULATOR CONTROL UNIT
RECORDER
ATTENUATOR
PHASE SHIFTER
BRIDGE ARM
TO MODULATOR IN SIGNAL CALIBRATOR
FREQUENCY MARKERS

Figure I.

3.3 Frequency Measurements

Rotational transition frequency measurements were made with the Hewlett-Packard spectrometer and recorder display.

There are several methods one can use to measure the frequency of an MRR absorption line. The method used will depend on the line strength, width, and accuracy desired by the operator. The spectrometer has an accuracy of 1 KHz. However, if the lines are weak or broad, it may not be possible to report a frequency measurement to 1 KHz.

The method used in this work for measuring lines (both narrow and broad) was to sweep up and down over the line at the same rate. The frequency from both traces was extracted from the markers and averaged. By taking the average, any frequency displacement due to the time constant and marking system is eliminated.

3.4 Complete Spectrometer Systems

An integrated spectrometer system for the 8.2-12.4 GHz, 12.4-18 GHz, 18-26.5 GHz, and 26.5-40 GHz regions has been described and is marketed commercially by the Hewlett-Packard company. The last two of the above frequency bands are available at this laboratory. This spectrometer employs a BWO source whose frequency is indicated continuously on a digital meter. The frequency can be adjusted manually or scanned automatically over any range. The frequency sweep rates are 1, 0.1, 0.01, and 0.001 MHz/sec. The above sweep

rates can be increased by factors of 10, 5, 2, and 1.

The spectrometer is well suited for quantitative determinations, particularly relative intensity measurements.

IV. METHYLDIFLUOROPHOSPHINE BORANE

4.1 Introduction

A microwave study of two isotopic species of methyldifluorophosphine borane, $CH_3PF_2{}^{11}BH_3$, and $CH_3PF_2{}^{11}BD_3$, was undertaken as a result of the recent interest in the structural and bonding aspects of substituted difluorophosphines (39-46). The structure of this compound is related closely to that of difluorophosphine borane (45) and methyldifluorophosphine (42). It is also related to several fluorophosphine and phosphorus boron adducts with known structures. A study of methyldifluorophosphine borane showed no splittings in the ground state rotational transitions due to boron quadrupole or internal rotation. Therefore, high barriers to internal rotation are expected for both the methyl and the borane tops in methyldifluorophosphine borane. For methyldifluorophosphine the barrier to internal rotation was reported to be greater than 3600 cal/mole, while for difluorophosphine borane the barrier was estimated as 3600-4500 cal/mole.

The two species $CH_3PF_2BH_3$, and $CH_3PF_2BD_3$, were prepared (47) by reacting CH_3PF_2 with B_2H_6 and B_2D_6 respectively. The rotational spectrum was observed at both room and dry ice temperature.

4.2 Spectrum

The preliminary structural parameters of methyldifluorophosphine borane were transferred from difluorophosphine borane (45). The rotational constants were calculated by means of the STRUCT computer program. The resulting molecular parameters, and moments of inertia for the two species $CH_3PF_2BH_3$, and $CH_3PF_2BD_3$ are given in Table 2. The projection of the molecule on the molecular symmetry plane, the a-b inertial plane, is shown in Figure II. Since the c axis is perpendicular to the molecular plane of symmetry, the c component of the dipole moment, μ_c, will be zero; therefore only a- and b-type transitions should be observed.

The spectrum of each species is very rich, with transitions practically every few MHz. The strongest transitions occur in bands extending over about 1300-1500 MHz and containing more than 50 lines. Calculations, based on a preliminary structure, indicated that these transitions were ground-state Q-band transitions, b-type, of a slightly asymmetric prolate top. These transitions correspond in the symmetric top limit to those of the type $K_{-1} \rightarrow K_{-1} + 1$, $J \rightarrow J$, with the lines of a given band having the same value of K_{-1}. In each band the spacing between successive transitions decreases as the frequency increases; this gives rise to a characteristic clustering of lines at the high frequency edge, or band head.

Table 2. Assumed structural parameters and rotational parameters of $CH_3PF_2{}^{11}BH_3$, and $CH_3PF_2{}^{11}BD_3$.

r(PF)	1.552 Å	< (FPF)	100.0°
r(PB)	1.832	< (FPB)	115.47°
r(PC)	1.834	< (FPC)	101.45°
$r(BH_s)$	1.20	< (BPC)	120.0°
$r(BH_a)$	1.226	< (H_aBH_a)	112.69°
r(CH)	1.093	< (HCH)	109.19°

Rotational constants (MHz) and moments of inertia (amu. Å^2).

	$CH_3PF_2BH_3$	$CH_3PF_2BD_3$
A	4185.7	4024.1
B	3630.3	3251.1
C	3482.2	3119.1
I_a	120.7	125.5
I_b	139.2	155.4
I_c	145.1	162.0
κ	-0.578	-0.708

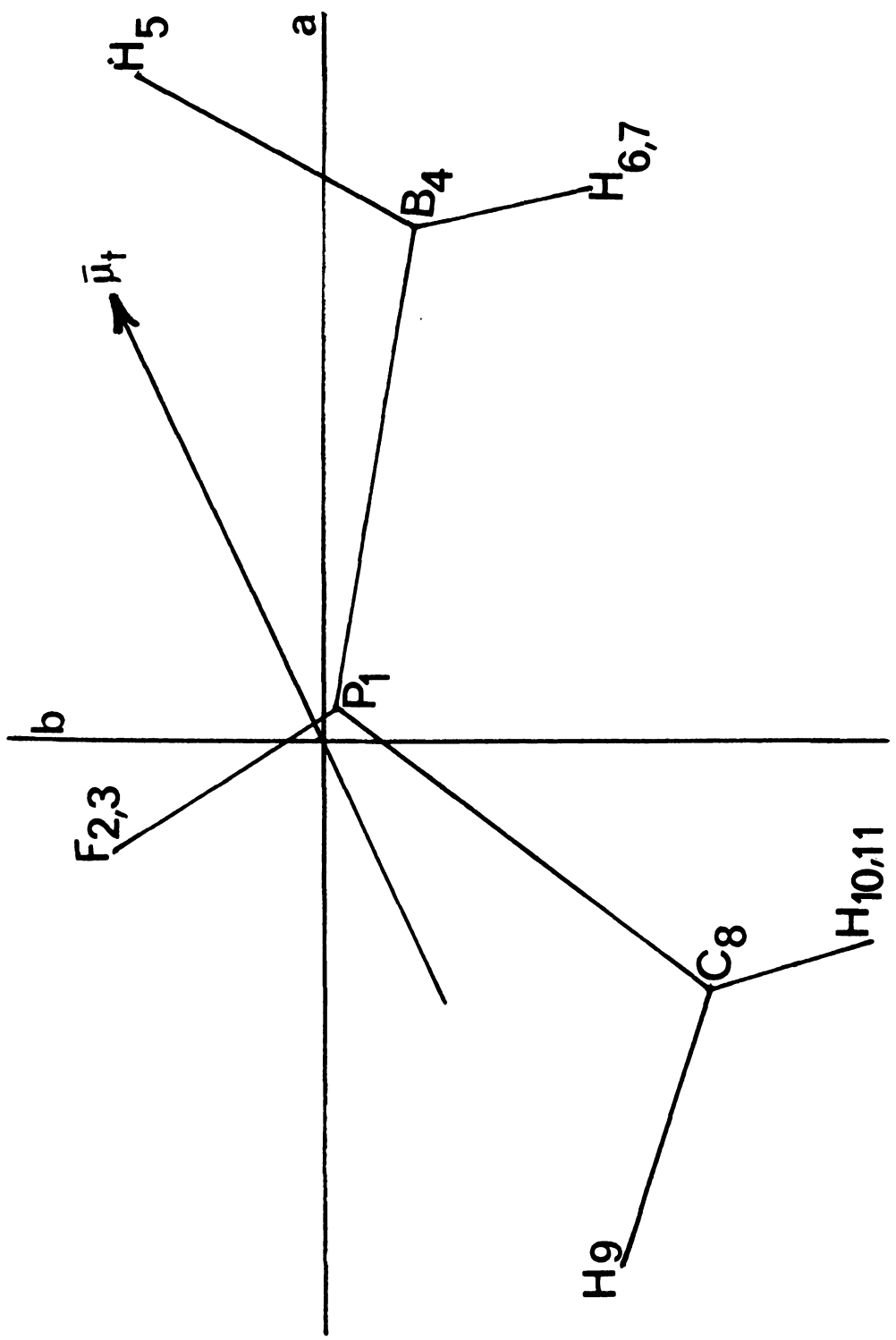

Figure II. Projection of $CH_3PF_2BH_3$ onto the molecular symmetry plane. The orientation of the dipole moment vector, $\bar{\mu}_t$, is also shown.

The K_{-1} quantum numbers of the bands are easily determined from the positions of the band heads which are not much affected by rotational asymmetry. The spacing between successive band heads is almost constant throughout the recorded region (18 - 40 GHz) for the two species. This spacing, which is about twice the value of (A - (B + C)/2), was found to be 1240 MHz for methyldifluorophosphine- $^{11}BH_3$, and 1700 MHz for $CH_3PF_2{}^{11}BD_3$. These values were very sensitive to the structural parameters, which were varied until they could be reproduced for both species. The rotational constants obtained from the structure are the ones shown in Table 2; they were used to calculate rotational energy levels and transition frequencies. These calculations were done by means of the computer program EIGVALS (48). The required input data for the EIGVALS program are the rotational constants, quadrupole coupling constants and dipole moments. The program calculates the rotational energy levels, quadrupole coupling energies, transition frequencies, line strengths, Stark effect coefficients, and Stark shifts for a rigid asymmetric rotor. The intensity and Stark effect for any rotational transition are extremely important for spectral assignments. Transition intensities are calculated from line strength (49,50), while Stark effects are calculated from Stark coefficients which are calculated by second-order perturbation theory from the line strengths and energy levels.

A search of spectral regions predicted by EIGVALS disclosed groups of transitions which were approximately separated by (B + C) as expected for a-type transitions. Both a- and b-type transitions were observed. The observed and calculated frequencies of the assigned transitions for the two species are compared in Tables 3 - 6, while the rotational parameters from the rigid rotor fits are presented in Table 7. The assignment of the transitions in the two species were verified by the Stark effect, relative intensities, frequency fit, and expected isotope shift. The spectrum of the ^{10}B species in natural abundance was predicted to lie in very rich regions and unfortunately a-type transitions could not be identified for either ^{10}B species.

The high J —> J, Q-branch transitions were fit for both species by using the computer program CDFIT which was written by R. H. Schwendeman. This program fits the observed assigned transitions by the method of least squares. It uses a model Hamiltonian including rigid rotor and quartic centrifugal distortion terms. It was observed that a good fit (standard deviation = 0.28 MHz) was obtained when fitting any one of the Q-branches with the low J R-branch transitions. However, the standard deviation increased to 1.92 MHz when a fit including two Q-branches was attempted. This suggests that sextic distortion parameters are important. The eight adjusted molecular parameters, three rotational constants and five centrifugal-distortion parameters, are given in Table 8.

Table 3. Observed and calculated frequencies[a] of ground state rotational transitions for $CH_3PF_2{}^{11}BH_3$.

Transition	ν_{obs}	ν_{calc}	$\Delta\nu$[b]
$2_{11} - 3_{12}$	21708.13	21708.91	-0.78
$3_{03} - 4_{04}$	28429.50	28429.40	0.10
$3_{13} - 4_{14}$	28315.10	28314.82	0.28
$4_{04} - 5_{15}$	35517.30	35517.57	-0.27
$4_{13} - 5_{14}$	36056.32	36056.31	0.01
$4_{14} - 5_{15}$	35359.37	35359.26	0.10
$4_{04} - 5_{05}$	35435.04	35435.0	0.04
$4_{23} - 5_{24}$	35771.50	35771.66	-0.16
$4_{32} - 5_{33}$	35901.09	35901.17	-0.08
$4_{31} - 5_{32}$	35965.69	35965.80	-0.11
$4_{22} - 5_{23}$	36168.38	36168.16	0.21

[a] In MHz; estimated uncertainty in observed transitions ±0.05 MHz. Rigid rotator parameters used to calculate frequencies are in Table 7.

[b] $\Delta\nu = \nu_{obs} - \nu_{calc}$.

Table 4. Observed and calculated frequencies[a] of ground state rotational transitions for $CH_3PF_2{}^{11}BD_3$.

Transition	ν_{obs}	ν_{calc}	$\Delta\nu$[b]
$2_{02} - 3_{03}$	19139.0	19138.31	0.68
$3_{13} - 4_{14}$	25312.0	25312.37	-0.37
$3_{22} - 4_{23}$	25580.65	25581.04	-0.39
$3_{03} - 4_{04}$	25459.72	25459.31	0.41
$3_{12} - 4_{13}$	25814.37	25814.56	-0.19
$4_{31} - 5_{42}$	37911.80	37911.88	-0.08
$5_{23} - 6_{24}$	38697.89	38697.34	0.54
$5_{33} - 6_{34}$	38440.92	38441.49	-0.57
$5_{24} - 6_{25}$	38324.65	38324.47	0.17
$5_{15} - 6_{16}$	37917.80	37917.61	0.18
$5_{14} - 6_{15}$	38627.44	38626.85	0.58
$5_{51} - 6_{52}$	38423.70	38423.91	-0.21
$5_{50} - 6_{51}$	38423.70	38423.95	-0.25
$5_{05} - 6_{06}$	38012.90	38013.11	-0.21
$5_{05} - 6_{16}$	38169.80	38169.75	0.04
$5_{24} - 6_{15}$	36970.60	36970.80	-0.20

[a] In MHz; estimated uncertainty in observed ±0.05 MHz. Rigid rotor parameters used to calculate frequencies are in Table 7.

[b] $\Delta\nu = \nu_{obs} - \nu_{calc}$.

Table 5. Observed and calculated Q-branch frequencies of ground state rotational transitions for $CH_3PF_2{}^{11}BH_3$.

Transition	ν_{obs} [a]	ν_{calc} [b]	$\Delta\nu$ [c]
$20_{15,6} - 20_{16,5}$	18725.90	18725.83	0.07
$22_{15,8} - 22_{16,7}$	18674.96	18674.85	0.10
$24_{15,10} - 24_{16,9}$	18607.85	18608.15	-0.30
$26_{15,12} - 26_{16,11}$	18522.45	18522.45	0.00
$28_{15,14} - 28_{16,13}$	18414.08	18413.90	0.17
$30_{15,16} - 30_{16,15}$	18277.90	18277.86	0.03
$22_{16,7} - 22_{17,6}$	19917.03	19916.37	0.65
$24_{16,9} - 24_{17,8}$	19860.11	19860.29	-0.18
$26_{16,11} - 16_{17,10}$	19788.30	19788.45	-0.15
$28_{16,13} - 18_{17,12}$	19697.85	19697.84	0.00
$30_{16,15} - 30_{17,14}$	19584.34	19584.94	-0.60
$32_{16,17} - 32_{17,16}$	19445.94	19445.57	0.36

[a] In MHz; estimated experimental uncertainty ±0.05 MHz.

[b] Calculated from rotational parameters given in Table 8.

[c] $\Delta\nu = \nu_{obs} - \nu_{calc}$.

Table 6. Observed and calculated Q-branch frequencies of ground state rotational transitions for $CH_3PF_2{}^{11}BD_3$.

Transition	ν_{obs} [a]	ν_{calc} [b]	$\Delta\nu$ [c]
$13_{11,3} - 13_{12,2}$	19418.30	19418.40	-0.10
$15_{11,5} - 15_{12,4}$	19395.70	19395.53	0.16
$17_{11,7} - 17_{12,6}$	19362.87	19362.82	0.04
$19_{11,9} - 19_{12,8}$	19317.55	19317.53	0.01
$21_{11,11} - 21_{12,10}$	19256.28	19256.47	-0.19
$23_{11,13} - 23_{12,12}$	19175.92	19175.86	0.05
$15_{12,4} - 15_{13,3}$	21098.94	21098.76	0.18
$16_{12,5} - 16_{13,4}$	21086.71	21086.58	0.12
$17_{12,6} - 17_{13,5}$	21072.70	21072.23	0.46
$19_{12,8} - 19_{13,7}$	21035.86	21035.93	-0.07
$21_{12,10} - 21_{13,9}$	20986.85	20987.45	-0.60
$23_{12,12} - 23_{13,11}$	20924.21	20924.04	0.16

[a] In MHz; estimated experimental uncertainty ±0.05 MHz.

[b] Calculated from rotational parameters given in Table 8.

[c] $\Delta\nu = \nu_{obs} - \nu_{calc}$.

Table 7. Ground state rotational parameters[a] of $CH_3PF_2{}^{11}BH_3$ and $CH_3PF_2{}^{11}BD_3$.

Parameter	$CH_3PF_2{}^{11}BH_3$	$CH_3PF_2{}^{11}BD_3$
A[b]	4194.60	4044.75
B	3659.57	3262.54
C	3507.23	3135.47
I_a[c]	120.4825	124.9459
I_b	138.0969	154.9026
I_c	144.0952	161.1801
P_{aa}[d]	80.8548	95.5684
P_{bb}	63.2404	65.6117
P_{cc}	57.2420	59.3342
κ	-0.55674	-0.72051

[a] Obtained from rigid rotator frequency fit.

[b] In MHz; uncertainty in the rotational constants is ±0.05 MHz.

[c] In u.Å^2 ; conversion factor: 505376 MHz u.Å^2.

[d] In u.Å^2 ; $P_{aa} = (I_b + I_c - I_a)/2$, etc.

Table 8. Ground state rotational, and centrifugal distortion parameters[a] for $CH_3PF_2{}^{11}BH_3$ and $CH_3PF_2{}^{11}BD_3$.

Parameter	$CH_3PF_2{}^{11}BH_3$	$CH_3PF_2{}^{11}BD_3$
A	4194.42	4044.68
B	3659.47	3262.55
C	3507.10	3135.50
D_J	-0.00288	0.00034
D_{JK}	-0.01099	0.00306
D_K	0.13447	-0.12395
D_{WJ}	0.01446	-0.00174
D_{WK}	-0.13736	0.11726

[a]In MHz; obtained from CDFIT program.

4.3 Molecular Structure

Two isotopic species were studied for methyldifluorophosphine borane. The molecular structure of the compound was found to be especially sensitive to the value of $(A - (B + C)/2)$, and great effort was expended to obtain a reasonable structure which gives the experimental value of $(A - (B + C)/2)$ for both species.

To obtain a molecular structure reasonable assumptions had to be made concerning some of the molecular parameters. The geometry of the methyl group was assumed to include

r(CH) = 1.093 Å and ∠ PCH = 109.75°. The borane group was assumed either tilted (45) away from the fluorine atoms or symmetric (46) with respect to the PB bond. Then, if the PF bond length is assumed, the remaining molecular parameters, r(PC), r(PB), ∠ (FPF), ∠ (FPC), ∠ (FPB), and ∠ (BPC), may be determined by a fit of the rotational parameters I_a, I_b, and I_c for both species.

The fitting was done by means of the computer program STRFIT written by Dr. R. H. Schwendeman. Table 9 shows a comparison between the calculated fitting parameters of the compound for both a tilted and a symmetric borane group. It was found that the calculated PC bond length and the FPF and BPC angles are quite sensitive to the assumed PF bond length. The FPF and BPC angles were found to be unreasonable for a PF distance greater than 1.55 Å or less than 1.54 Å. With the above PF bond distances and fixed methyl group geometry the structural parameters of the compound were tested for several symmetric borane groups. A series of calculations were carried out by assuming the BH bond distance equal to 1.19 Å, 1.20 Å, 1.21 Å, 1.22 Å, and 1.23 Å. The result of these calculations showed that the PC, PB bond lengths, and BPC angle are very sensitive to the BH bond distance. This appears to be a result of the proximity of the P atom to the center of mass. The most reasonable results are shown in Table 9, where the PF bond distance is assumed to be 1.55 Å and 1.54 Å for both tilted and symmetric borane groups. The PC and PB bond

Table 9. Comparison between the structural parameters of $CH_3PF_2BH_3$ for both tilted and symmetric borane groups.

Bond Angles and Bond Distances	Tilted BH_3		Symmetric BH_3	
P-F	1.54Å	1.55Å	1.54Å	1.55Å
P-C	1.799	1.779	1.669	1.649
P-B	1.863	1.863	1.993	1.995
∠ FPF	100.86°	99.97°	100.86°	99.97°
∠ BPC	117.25°	118.39°	118.56°	119.52°
∠ FPC	102.21°	102.67°	108.40°	108.83°
∠ FPB	115.92°	115.29°	109.57°	108.95°
B-H_a	1.226Å	1.226Å	1.20Å	1.20Å
B-H_s	1.20	1.20	1.20	1.20
∠ H_aBH_a	112.53°	112.53°	116.34°	116.34°
C-H	1.093Å	1.093Å	1.093Å	1.093Å
∠ HCH	109.19°	109.19°	109.19°	109.19°

distances obtained from the assumed symmetric borane group seem to be unsatisfactory, and consequently it is highly probable that the molecular structure has a tilted borane group although the tilt may not be quite that assumed. The Cartesian coordinates in the principal axis system for the structure with PF = 1.55Å and the tilted borane group are given in Table 10.

4.4 Dipole Moment

The shifts in the frequencies of the Stark components of transitions in $CH_3PF_2BH_3$, and $CH_3PF_2BD_3$ were measured as a function of electric field (E) in a Stark cell which was calibrated by measuring the Stark shifts in the J = 1-2 transition in OCS (μ_{OCS} = 0.7152D) (51). The resulting slopes for both species, $d\Delta\nu/dE^2$, were used with Eq. (2-21) to calculate the dipole moment components, μ_a and μ_b (μ_c = 0 by symmetry). The observed and calculated slopes for the two species along with the resulting dipole moments are given in Table 11. The data in Table 11 give values for $CH_3PF_2BH_3$ of $|\mu_a|$ = 3.52 D, $|\mu_b|$ = 1.765D, and $|\mu_t|$ = 3.95 ± 0.05 D, and for $CH_3PF_2BD_3$ values of $|\mu_a|$ = 3.50 D, $|\mu_b|$ = 1.95 D, and $|\mu_t|$ = 4.00 D. For $CH_3PF_2BH_3$ the angle between the a-axis and the dipole moment vector is 26.06°, while for $CH_3PF_2BD_3$ the angle is 29.13°. These angles require that the dipole moment vector be oriented as shown in Figure II. A comparison of the reported dipole moments for some difluorophosphine derivatives and phosphorus-boron adducts is given in Table 12.

Table 10. Cartesian coordinates for $CH_3PF_2{}^{11}BH_3$ in the principal axis system.[a]

Atom	a	b	c
P_1	0.1096	-0.0541	0.0000
F_2	-0.4328	0.7819	1.1871
F_3	-0.4328	0.7819	-1.1871
B_4	1.9521	-0.3354	0.0000
H_5	2.5263	0.7182	0.0000
H_6	2.0625	-1.0072	1.0195
H_7	2.0625	-1.0072	-1.0195
C_8	-0.9632	-1.4740	0.0000
H_9	-2.0066	-1.1485	0.0000
H_{10}	-0.7755	-2.0787	0.8908
H_{11}	-0.7755	-2.0787	-0.8908

[a]The coordinates shown here were calculated from the structural parameters given in Table 9; tilted borane group and PF = 1.55Å.

Table 11. Stark coefficients and dipole moments of $CH_3PF_2{}^{11}BH_3$ and $CH_3PF_2{}^{11}BD_3$.

Transition	M	$d\nu/dE^2$(obsd)[a,b]	Calcd
$CH_3PF_2{}^{11}BH_3$			
$4_{04} - 5_{05}$	±1	15.50	15.47
	±2	87.0	87.25
	±3	207.0	206.89
$4_{14} - 5_{15}$	±1	18.65	18.47
	±2	97.50	97.55
	±3	228.0	229.20
	$\mu_a = 3.52 \pm 0.05$ D		
	$\mu_b = 1.765 \pm 0.005$ D		
	$\mu_c = 0.0$ D		
	$\mu_t = 3.95 \pm 0.05$ D		
$CH_3PF_2{}^{11}BD_3$			
$3_{03} - 4_{04}$	0	-19.00	-19.00
	±1	64.40	64.40
	$\mu_a = 3.50 \pm 0.05$ D		
	$\mu_b = 1.95 \pm 0.01$ D		
	$\mu_t = 4.00 \pm 0.05$ D		

[a] In MHz/(kv/cm)^2, assuming $\mu_{OCS} = 0.7152$ D.

[b] Uncertainty in observed slopes is ±0.5%.

Table 12. Comparison of the dipole moments for some difluorophosphine derivatives and phosphorus-boron adducts.

Compound	μ_T [a]	Ref.
HPF_2	1.32	43
CH_3PF_2	2.056	42
$CH_3PH_2BH_3$	4.66	44
$(CH_3)_3PBH_3$	4.99	44
F_3PBH_3	1.64	46
HF_2PBH_3	2.5	45
$CH_3PF_2BH_3$	3.95	This Study

[a] In Debyes.

4.5 Discussion

Several results of the study of $CH_3PF_2BH_3$ are worth comparing to results of studies of related phosphorus-boron adducts. These are the effect of the coordination on bond distances and bond angles, the relative stability towards dissociation, and the large dipole moment.

Methyldifluorophosphine borane is related to several phosphorus-boron adducts as well as to difluorophosphine derivatives. If the structural parameters of CH_3PF_2 (42) are compared to those of the coordinated species, $CH_3PF_2BH_3$, the P-F bond length is smaller, while the FPF and FPC

angles are larger in the coordinated species. A similar effect is also evident upon comparison of the structural parameters of HF_2P with HF_2PBH_3 (45) and HF_2PO, which is isoelectronic with HF_2PBH_3.

In general, the data reported by Kuczkowski (43-46) reflect these two trends, namely bond lengths to phosphorus decrease and bond angles about phosphorus increase as more electronegative groups are attached. These trends can be rationalized by several semi-empirical models such as: 1) electron-pair repulsion (52), 2) hybridization changes, (53), 3) d orbital participation (54). Each of the preceding models incorporates the concept of electronegativity differences in order to rationalize systematic changes in structural parameters. The H_3B-X distance in different H_3B-X adducts has also been discussed in terms of orbital following and hyperconjugation in borane adducts (55). And, Percell (55) has applied the hybrid orbital force field (HOFF) of Mills (56) to these same trends.

The $CH_3PF_2BH_3$ addition compound is very stable at room temperature. It gave almost the same spectrum after being stored at room temperature for about two months. After three months or so a portion of the gaseous sample turned into liquid drops of very low vapor pressure. The short P-B bond is consistent with the stability of $CH_3PF_2BH_3$ towards dissociation to its component donor and acceptor molecules. Chemically, the stability of the compound is not surprising in view of the fact that CH_3PF_2 is considered a strong Lewis base.

The dipole moment of $CH_3PF_2BH_3$ (3.95 D) is considerably larger than that in HF_2PBH_3 (2.5 D). Similarly, a big difference in the dipole moment was reported for CH_3PF_2 (2.05 D) and PF_2H (1.32 D). Since the primary electronic effects of CH_3 and H are usually considered to be comparable, this is evidence of some unusual electronic effect in both $CH_3PF_2BH_3$ and CH_3PF_2.

Kuczkowski (43-46) has pointed out that coordination compounds tend, in general, to have rather large dipole moments, and $CH_3PF_2BH_3$ is no exception to this rule. The large moments are usually attributed to the appreciable bond-moment associated with the dative bond. The reported (44) P-BH_3 bond moment is approximately 3.4-4.0 D.

V. N-METHYLFORMAMIDE

5.1 Introduction

Compounds containing an N-C-O linkage characteristic of amides and polypeptides are important not only spectroscopically, but also biologically. Pauling (25) described the N-C-O bonding system in terms of two resonating forms, and suggested that the H_2N-C group is planar. This picture, in which the C-N bond has an appreciable partial double-bond character, has been supported by work in a number of fields (57-60).

In the first microwave investigation (26) of formamide, the simplest member of the above class of compounds, it was concluded that formamide is indeed planar in the gas phase. However, a more detailed study of the spectrum by Costain and Dowling (27) gave evidence that the molecule is non-planar with the H_2N-C group forming a shallow pyramid.

A proton NMR study of N-monosubstituted aliphatic amides in solution showed that the configuration, in which the alkyl substituent is *cis* to the carbonyl oxygen, is predominant (61), and that the percentage of the *trans* conformer increases slightly as the nitrogen substituent becomes more bulky. The percent *cis* conformer decreases from 92% for N-methylformamide to 88% for N-ethylformamide

and N-isopropylformamide (62). Studies of vibrational spectra of geometrical isomers in amides (63) have also shown that the majority of the N-monosubstituted amides exist predominantly in the cis form.

A microwave study of N-methylformamide, CH_3NHCHO, was undertaken in response to the current interest in the structural and bonding aspects of substituted amides. The preferred configuration has been shown to be the one in which the N-methyl group is cis to the carbonyl oxygen as in Figure III. Unfortunately, it was not possible to assign a spectrum to the trans species. This is consistent with the results of the nmr and ir studies mentioned above. The barrier to internal rotation, the nuclear quadrupole coupling constants, and the dipole moment were determined for the cis species. The rotational spectrum was observed at both room and dry ice temperature.

5.2 Spectrum

The preliminary structural parameters of N-methylformamide were transferred from formamide (27). The rotational constants were calculated with the STRUCT computer program. The molecular parameters, atomic coordinates, and moments of inertia for cis N-methylformamide are given in Tables 13 and 14. The molecule is predicted to have an a-b inertial plane of symmetry. Therefore, only a and b-type transitions should be observed.

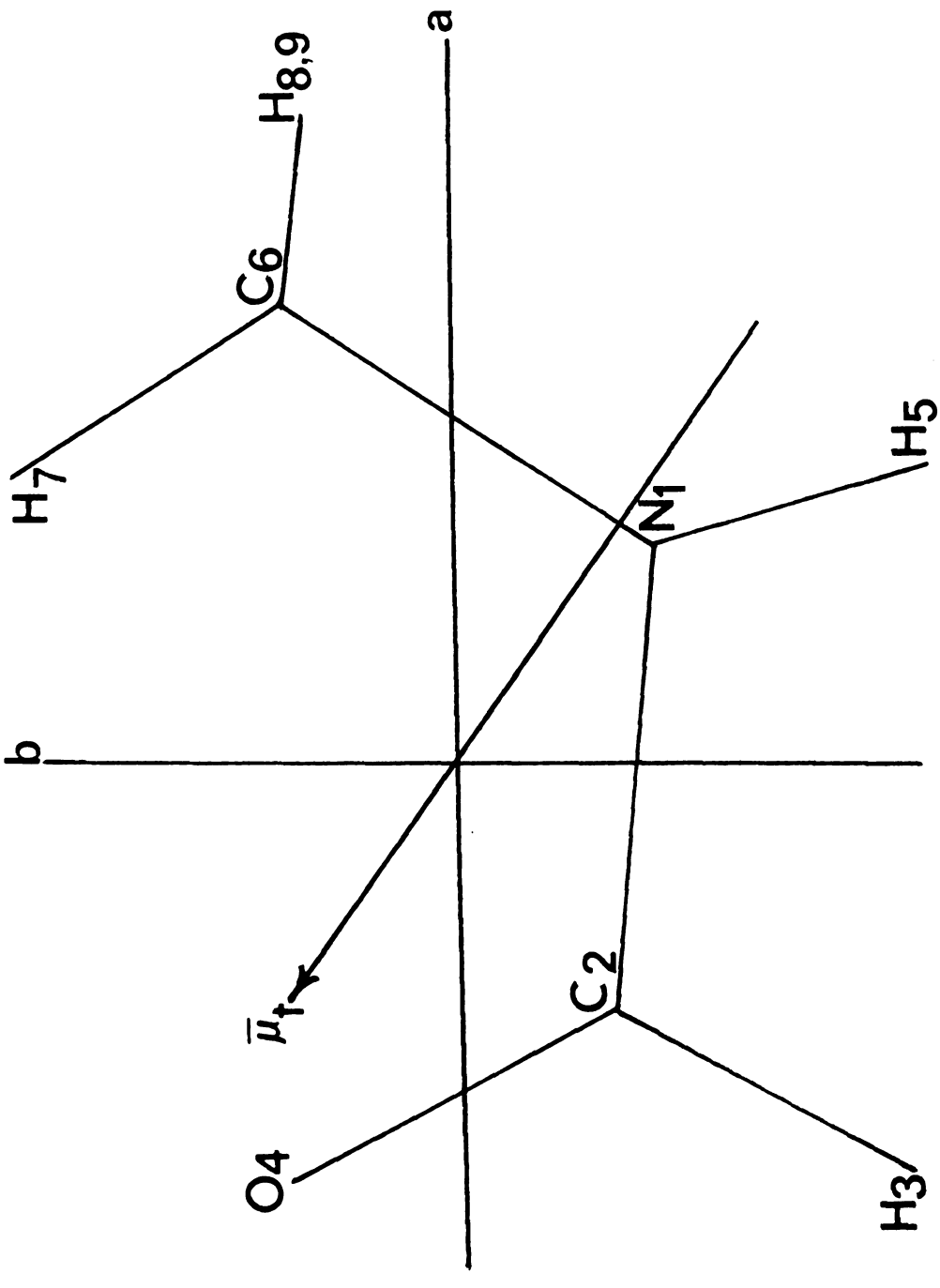

Figure III. Projection of N-methylformamide onto the molecular symmetry plane. The probable orientation of the dipole moment vector, $\bar{\mu}_t$, is also shown.

Table 13. Assumed structural and rotational parameters of cis N-methylformamide.

$r(NC_2)$	1.376 Å	$\angle$ NCO	124.0°
$r(NC_6)$	1.470	$\angle$ NCH	113.0°
$r(NH_5)$	1.0	$\angle$ CNH	119.0°
$r(CH)$	1.093	$\angle$ OCH	123.0°
$r(C_2O)$	1.193	$\angle$ CNC	122.7°

Rotational constants (MHz) and moments of inertia ($u.Å^2$)

	cis N-Methylformamide
A	19851.39
B	6125.00
C	4824.19
I_a	25.45
I_b	82.51
I_c	104.75
κ	-0.82

Table 14. Cartesian coordinates for cis N-methylformamide in the principal axis system.[a]

Atom	a	b	c
N_1	0.5769	-0.6342	0.0000
C_2	-0.7905	-0.4814	0.0000
H_3	-1.3267	-1.4339	0.0000
O_4	-1.3438	0.5754	0.0000
H_5	0.9503	-1.5618	0.0000
C_6	1.5034	0.5070	0.0000
H_7	0.9335	1.4396	0.0000
H_8	2.1333	0.4655	0.8922
H_9	2.1333	0.4655	-0.8922

[a]The coordinates shown above were calculated from the assumed structural parameters given in Table 13. The coordinates are in Å.

The spectrum calculated by the EIGVALS computer program from the assumed parameters served as a guide in the initial search for an assignment. An assignment was made by observing the characteristic Stark effect of several low J R-branch a and b-type transitions. Transitions in the Q-branch series $J_{0,J} - J_{1,J-1}$, were also identified by their resolvable Stark effect and quadrupole hyperfine splittings. A Q-branch plot for both series is shown in Figure IV.

The graphical values of $(A-C)/2$ and (κ) agree well with those obtained by numerical fitting of the rotational frequencies. After it was realized that the transitions in N-methylformamide were widely split by internal rotation of the methyl group, these transitions were assigned to the levels of A symmetry of the internal rotations. The observed assigned A-level transitions, corrected for quadrupole hyperfine splittings, are compared with calculated values in Table 15. The comparison shows considerable deviation from the rigid-rotor frequencies which is attributed to the internal rotation of the methyl group. The corresponding effective rotational parameters of the A-level transitions are given in Table 16.

A good fit for A-level transitions was obtained by using the CDFIT computer program including centrifugal distortion parameters. The result of this fitting and the adjusted eight molecular parameters are given in Tables 17 and 18, respectively. The parameters of Table 16 give a very small out-of-plane second moment of inertia P_{cc}. The

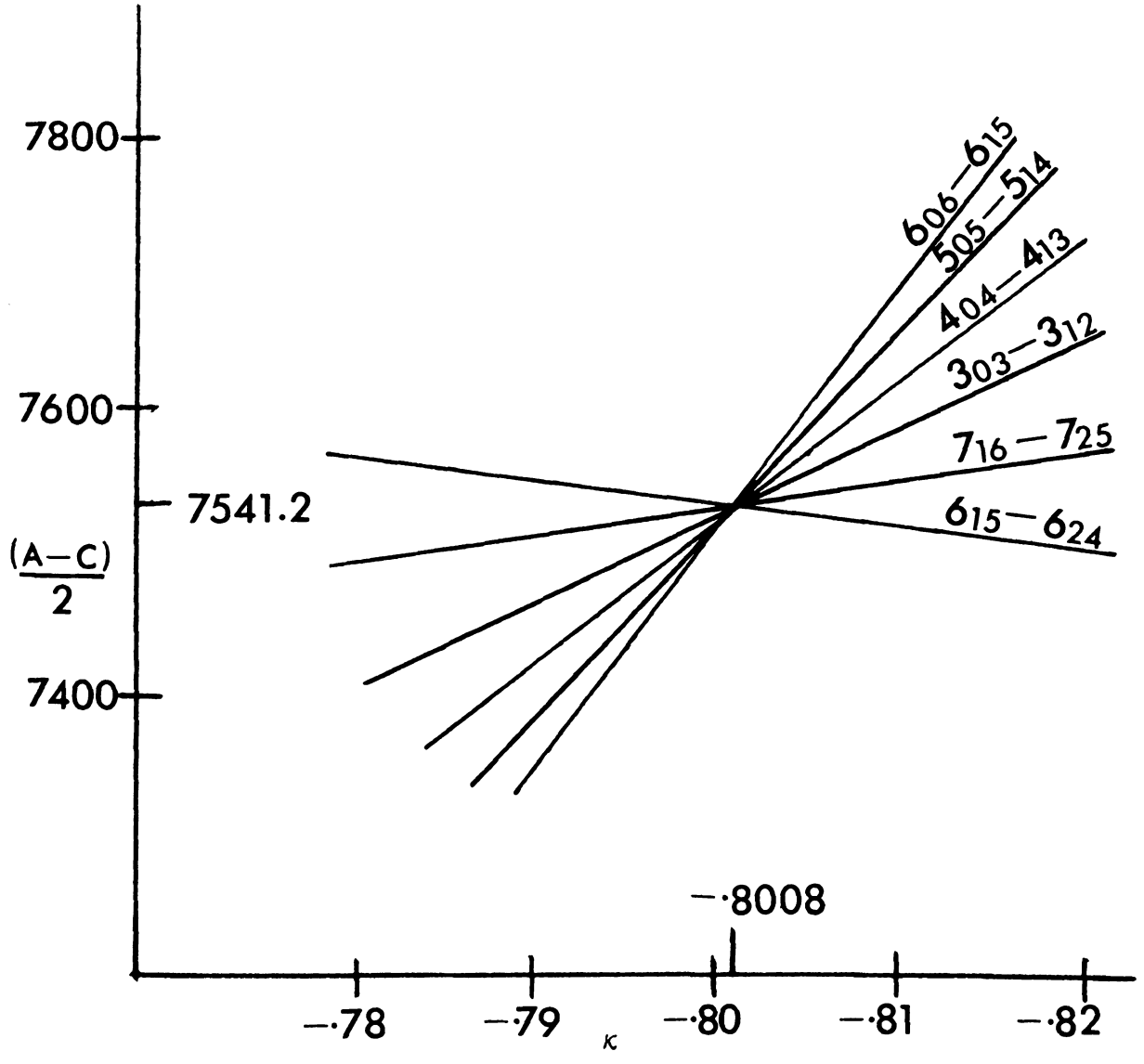

Figure IV. Plots of (A - C)/2 vs. κ for cis N-methylformamide

Table 15. Experimental hypothetical unsplit frequencies for cis N-methylformamide (A species).

Transition	ν_{exp}[a] MHz	ν_{calc}[b] MHz	Deviation MHz
$0_{00} \rightarrow 1_{11}$	24888.80	24888.43	0.36
$1_{10} \rightarrow 2_{11}$	24116.43	24116.45	-0.02
$1_{01} \rightarrow 2_{12}$	34694.67	34694.67	-0.00
$1_{11} \rightarrow 2_{12}$	21112.71	21113.80	-1.09
$2_{12} \rightarrow 3_{03}$	21259.79	21259.31	0.47
$2_{02} \rightarrow 3_{03}$	33455.90	33456.57	-0.67
$2_{11} \rightarrow 3_{12}$	36097.17	36097.99	-0.82
$3_{13} \rightarrow 4_{04}$	33755.03	33753.80	1.23
$3_{03} \rightarrow 3_{12}$	19343.51	19342.65	0.85
$4_{04} \rightarrow 4_{13}$	23228.42	23227.62	0.79
$5_{05} \rightarrow 5_{14}$	28566.61	28566.24	0.36
$6_{06} \rightarrow 6_{15}$	35466.23	35467.08	-0.85

[a] Corrected from observed frequencies by using the quadrupole parameters in Table 21.

[b] Calculated by using the rotational constants given in Table 16.

Table 16. Ground state rotational parameters for cis N-methylformamide (A species).

Parameter	V = 0
A (MHz)	19985.315
B	6404.443
C	4903.119
I_a (u.Å^2)	25.2873
I_b	78.9102
I_c	103.0723
P_{aa}[a] (u.Å^2)	78.3475
P_{bb}	24.7247
P_{cc}	0.5626
κ	-0.8009

[a] $P_{aa} = (I_b + I_c - I_a)/2$, etc.

Table 17. Observed and calculated ground state rotational transitions for cis N-methylformamide (A species).

Transition	ν_{obs} [a]	ν_{calc} [b]	$\Delta\nu$ [c]
$0_{00} \rightarrow 1_{11}$	24888.73	24888.20	-0.47
$1_{11} \rightarrow 2_{12}$	21112.49	21112.35	0.13
$1_{01} \rightarrow 2_{02}$	22497.38	22497.28	0.09
$1_{10} \rightarrow 2_{11}$	24116.33	24116.20	0.12
$1_{01} \rightarrow 2_{12}$	34694.50	34694.00	0.50
$2_{11} \rightarrow 3_{12}$	36097.21	36097.31	-0.10
$2_{21} \rightarrow 3_{22}$	33917.80	33917.88	-0.08
$2_{02} \rightarrow 3_{03}$	33455.83	33456.11	-0.28
$2_{12} \rightarrow 3_{13}$	31597.60	31597.76	-0.16
$3_{03} \rightarrow 3_{12}$	19343.86	19343.79	0.06
$3_{13} \rightarrow 4_{04}$	33755.09	33754.92	0.17
$4_{13} \rightarrow 4_{22}$	37428.39	37428.42	-0.03
$4_{04} \rightarrow 4_{13}$	23228.82	23228.32	0.49
$5_{05} \rightarrow 5_{14}$	28565.32	28565.95	-0.63
$6_{06} \rightarrow 6_{15}$	35464.92	35464.70	0.21
$6_{15} \rightarrow 6_{24}$	35714.0	35713.99	0.00
$7_{16} \rightarrow 7_{25}$	36481.94	36481.88	0.05
$8_{17} \rightarrow 8_{26}$	38728.93	38728.96	-0.03

[a] In MHz; estimated experimental uncertainty ±0.05 MHz.

[b] Calculated from rotational parameters given in Table 18.

[c] $\Delta\nu = \nu_{obs} - \nu_{calc}$.

Table 18. Ground state rotational, and centrifugal distortion parameters[a] for cis N-methylformamide (A species).

Parameter	v = 0
A	19987.553
B	6405.127
C	4902.444
D_J	0.0042
D_{JK}	0.0400
D_K	- 5.3149
D_{WJ}	0.1422
D_{WK}	6.0625

[a]In MHz; obtained from CDFIT program.

expected value (1.6 u.Å^2) is much larger than the value in Table 16 (0.562 u.Å^2).

The departure of the spectrum from a rigid-rotor fit, and small P_{cc} value indicated an effect of a low frequency vibration (64). On the assumption that the anomalous value for P_{cc} was caused by the internal rotation of the methyl group, the value of the potential barrier which would correct P_{cc} to the expected value was calculated (assuming that the molecule possesses a planar skeleton).

5.3 Barrier to Internal Rotation

A low barrier hindering the internal rotation of the methyl group in cis N-methylformamide produced very large splittings between A and E levels. To account for these splittings the matrix $H_{v\sigma}$ was calculated from Eq. (2-28) including perturbation coefficients to fourth order.

$$H_{v\sigma} = H_r + F \sum_{n=1}^{4} W_{v\sigma}^{(n)} \rho^{(n)} \qquad (2\text{-}28)$$

The matrix obtained from the above equation factors into blocks of dimension $2J + 1$ for each J. The matrix was diagonalized and the eigenvalues were calculated by means of the computer program INROT.

The barrier to internal rotation was predicted to be so low that the validity of the perturbation method used by the INROT program was in doubt. Therefore, the calculation was repeated with the FREEROT computer program which uses a low-barrier approximation in which free-rotor wave

functions form the basis set for the torsion of the methyl group (65). The required input data for the FREEROT program are the three-fold barrier height (V_3), the moment of inertia of the internal rotor about its symmetry axis (I_α), the angle between the symmetry axis of the internal rotor and the principal axis (θ), and the rigid rotor rotational constants A_0, B_0, and C_0.

For N-methylformamide

$$A_0 \cong A_A - \alpha^2 FW_{OA}^{(2)}, \quad B_0 \cong B_A - \beta^2 FW_{OA}^{(2)}, \quad C_0 = C_A.$$

A preliminary calculation was carried out with the effective second moments of inertia obtained from the A-level frequency fit and by using the above relations an approximate barrier height, V_3 = 190 cal/mole, was obtained. With this barrier height and calculated values of the other five rotational parameters the FREEROT program was used to predict the frequencies of the E transitions. The E-level transitions were then found and finally assigned through their characteristic first order Stark effect.

Final values of the internal rotation parameters were determined from a least-squares fit of 12 measured frequencies, six A-level and six E-level. The molecule was assumed to have a plane of symmetry such that the direction cosine, λ_c, between the methyl group axis and the out-of-plane C axis was zero. It was further assumed that the A-E splittings would vary linearly with the various parameters P_i,

$$\delta\Delta\nu = \sum_i \left(\frac{\partial\Delta\nu}{\partial P_i}\right)\delta P_i \ .$$

The derivatives $(\partial\Delta\nu/\partial P_i)$ were obtained numerically by varying each parameter individually and noting the effect on the $\Delta\nu$'s. The results of the calculation are given in Tables 19 and 20. In tables 19 and 20 the results of two calculations are shown. In one calculation the methyl group moment of inertia was allowed to vary and finally settled at the rather small value of 3.04 u.Å^2. In the second calculation I_α was fixed at the more reasonable value of 3.16 u.Å^2. The results show that the values of the barrier height are so close that it can be reported as $V_3 = 200 \pm 10$ cal/mole.

5.4 Nuclear Quadrupole Coupling Constants

The majority of molecules have no electronic angular momentum. If any hyperfine structure of rotational transitions is observed, it is therefore usually (66) due to the interaction between a nuclear quadrupole moment and the gradient of the electrical field produced at this nuclear position by the remaining molecular charges. The interaction of the quadrupole moment of the ^{14}N nucleus of the N-methylformamide with the electrical field gradient produces a hyperfine structure in certain transitions. This interaction causes the respective nuclear spin $\bar{I}$ and the molecular rotation $\bar{J}$ to couple to a resultant $\bar{F}$. The analysis of the rotational spectrum in the microwave region

Table 19. Comparison of observed and calculated transition frequencies for cis N-methylfomrmamide.

Transition	ν_{obs} [a]	$(\nu_{obs}-\nu_{calc})$ [b]	$(\nu_{obs}-\nu_{calc})$ [c]
	A Species		
$2_{11} \rightarrow 3_{12}$	36097.21	2.85	-2.45
$1_{11} \rightarrow 2_{12}$	21112.49	-6.95	-9.71
$1_{01} \rightarrow 2_{02}$	22497.38	-3.30	-6.55
$2_{21} \rightarrow 3_{22}$	33917.80	-2.60	-6.86
$3_{13} \rightarrow 4_{04}$	33755.09	2.24	1.65
$2_{20} \rightarrow 3_{21}$	34384.25	0.63	-3.47
	E Species		
$2_{11} \rightarrow 3_{12}$	34636.67	-7.97	-0.24
$1_{11} \rightarrow 2_{12}$	22423.50	8.63	10.83
$1_{01} \rightarrow 2_{02}$	21354.50	8.86	5.59
$2_{21} \rightarrow 3_{22}$	34227.45	-1.32	-2.29
$3_{13} \rightarrow 4_{04}$	34210.93	-2.53	-2.22
$2_{20} \rightarrow 3_{21}$	33798.85	4.00	16.27

[a] In MHz; observed frequencies.

[b] Obtained by using parameters in Table 20 with $I_{\alpha} = 3.04$ u.Å^2.

[c] Obtained by using parameters in Table 20 with $I_{\alpha} = 3.16$ u.Å^2.

Table 20. Rotational constants, and internal rotation parameters for cis N-methylformamide.

Effective Rotational Constants

A	= 19.98531 GHz
B	= 6.40444 GHz
C	= 4.90311 GHz

Internal Rotation Parameters

I_α	=	3.16 u.Å^2 [a]	I_α	=	3.04 u.Å^2 [b]
A_0	=	19.4755 GHz	A_0	=	19.4843 GHz
B_0	=	6.3289 GHz	B_0	=	6.3301 GHz
C_0	=	4.9053 GHz	C_0	=	4.9048 GHz
α	=	0.078149	α	=	0.075244
β	=	0.030350	β	=	0.029276
F	=	172.60297 GHz	F	=	178.59683 GHz
V_3	=	199.50 cal/mole	V_3	=	204.95 cal/mole
θ	=	50.07^0	θ	=	50.13^0
S	=	5.387	S	=	5.349

[a] Parameters obtained from least squares fit with I_α fixed at 3.16 u.Å^2.

[b] Parameters obtained from least squares fit with I_α varied.

including the hfs yields besides the rotational constants of the molecule the nuclear quadrupole coupling parameters. The hyperfine splittings in ^{14}N are of the order of one to two MHz; therefore, a first-order correction to the rigid-rotor Hamiltonian should be quite adequate.

$$H = H_r + H_Q \tag{5-1}$$

where H_Q that appears above is the correction term. For the frequency of any transition this correction may be written as

$$\Delta\nu_{quad} = \Delta\alpha\chi_{aa} + \Delta\beta(\chi_{bb} - \chi_{cc}) \tag{5-2}$$

where $\Delta\alpha$ and $\Delta\beta$ are functions of the inertial asymmetry, and the χ's are the quadrupole coupling constants referred to the principal inertial axis system. The coupling constants in the principal axis system of the quadrupole tensor, χ_{xx}, χ_{yy}, and χ_{zz} are related to those in the principal inertial axis system by a single parameter which may be taken to be the angle between the C_2N_1 bond (z-axis) and the a-axis, θ_{az}. If the y axis is taken to be parallel to the out-of-plane C principal axis, the relations are

$$\chi_{zz} = (\chi_{aa}\cos^2\theta_{az} - \chi_{bb}\sin^2\theta_{az})/(\cos^2\theta_{az} - \sin^2\theta_{az})$$

$$\chi_{xx} = (\chi_{aa}\sin^2\theta_{az} - \chi_{bb}\cos^2\theta_{az})/(\sin^2\theta_{az} - \cos^2\theta_{az})$$

$$\chi_{yy} = \chi_{cc} \tag{5-3}$$

The values of the χ's together with the transitions used in the least-square fit are given in Table 21.

Table 21. Frequencies of transitions used in the determination of the nuclear quadrupole coupling constants for cis N-methylformamide.

Transition	F → F'	ν_{obs} [a]	ν_{calc} [b]
$3_{03} \rightarrow 3_{12}$	4 → 4	19343.84	19343.83
	3 → 3	19342.43	19342.42
	2 → 2	19344.32	19344.33
$4_{04} \rightarrow 4_{13}$	5 → 5	23228.71	23228.71
	4 → 4	23227.22	23227.21
	3 → 3	23229.09	23229.09
$5_{05} \rightarrow 5_{14}$	6 → 6	28567.05	28567.02
	5 → 5	28565.32	28565.29
$6_{06} \rightarrow 6_{15}$	7 → 7	35466.71	35466.50
	6 → 6	35464.92	35464.72

Quadrupole Coupling Constants

χ_{aa} [c]	= 2.72 MHz	χ_{zz}	= 2.73 MHz
χ_{bb}	= 1.57 MHz	χ_{xx}	= 1.55 MHz
χ_{cc}	= -4.29 MHz	χ_{yy}	= -4.29 MHz
θ_{az}	= 6.34°		

[a] In MHz.

[b] ν_{calc} = the hypothetical unsplit frequency plus the hyperfine quadrupole splitting.

[c] $\chi_{aa} = eQ\,(\partial^2 v/\partial a^2)$, etc.

5.5 Dipole Moment

The shifts in the frequencies of seven Stark components of four transitions in N-methylformamide were measured as a function of electric field (E) in a Stark cell which was calibrated by measuring the Stark shifts in the $J = 1 \rightarrow 2$ transitions in OCS ($\mu_{OCS} = 0.7152$D) (51). The Stark coefficients for these transitions were computed by neglecting the small quadrupole interaction. The resulting seven slopes, $d\Delta\nu/dE^2$, were used with Eq. (2-21) to calculate the dipole moment components, μ_a and μ_b ($\mu_c = 0$ by symmetry). These slopes were also fit by least-squares and the observed and calculated results along with the resulting value of the dipole moment are given in Table 22. These data give values for N-methylformamide of $|\mu_a| = 2.95$ D, $|\mu_b| = 2.48$ D and $|\mu_t| = 3.86 \pm 0.02$ D. For N-methylformamide the angle between the a-axis and the dipole moment vector is (40.05^0). Although the sign of the dipole moment and the sign of the angle are not determined by these data, the most probable orientation makes an angle of 33.7^0 with the C-N bond and is directed as shown in Figure III.

5.6 Discussion

Interpretation of the relatively low barrier to internal rotation in cis N-methylformamide should take into account the following:

Table 22. Stark coefficients and dipole moment of cis N-methylformamide.

Transition	M	$(d\nu/dE^2)_{obs}$ [a]	$(d\nu/dE^2)_{calc}$ [a]
$0_{00} \rightarrow 1_{11}$	0	332.33	326.76
$1_{01} \rightarrow 2_{02}$	0	-68.50	-66.32
	1	258.0	259.65
$1_{10} \rightarrow 2_{11}$	0	119.0	117.54
	1	-1714.0	-1717.99
$1_{11} \rightarrow 2_{12}$	0	105.88	103.88
	1	1830.0	1831.08

$\mu_a = 2.95 \pm 0.02$ D

$\mu_b = 2.48 \pm 0.01$ D

$\mu_c = 0.0$

$\mu_t = 3.86 \pm 0.02$ D

[a] In MHz/(KV/cm)^2, assuming $\mu_{OCS} = 0.7152$ D.

(1) By comparison with the barrier height determined for methylamine (V_3 = 1976 cal/mole (67)) the H_3CNH fragment should give rise to a contribution to the barrier of about 1 kcal/mole favoring a configuration in which the methyl group staggers the NH bond.

(2) The contribution of the H_3CNC fragment to the barrier height is not easy to predict. The barriers to internal rotation in $H_3C-N=CH_2$ (68) and $H_3C-N=CH(CH_3)$ (69) are 1970 cal/mole, and 2109 cal/mole, respectively. In neither case, however was the equilibrium configuration of the methyl group determined. The barrier to internal rotation in dimethylamine (70) is 3200 cal/mole presumably favoring a staggered configuration. Thus, in addition to not knowing whether to consider the amide NC bond as a single or double bond, we do not have sufficient information on barrier heights of methyl groups attached to nitrogen.

(3) In the configuration in which the methyl group in cis N-methylformamide staggers the NH bond the distance between one of the hydrogen atoms of the methyl group and carbonyl oxygen is less than the sum of the van der Waals' radii (2.60 Å) for the two atoms. In the eclipsed configuration the distance is larger (Fig. 5).

It has been shown in a large number of cases that a severe effect on the barrier to internal rotation occurs whenever atoms approach distances which are smaller than the sum of the van der Waals' radii. The magnitude of this effect has been shown to be 1-2 kcal/mole which can either increase or decrease the barrier height depending on whether the steric hindrance occurs when the methyl is in its low energy or high energy configuration, respectively.

The result of this discussion is that interpretation of the low barrier in cis N-methylformamide is very difficult in the light of the present knowledge of barrier heights in nitrogen compounds. It is made particularly difficult by the lack of knowledge of equilibrium configuration of the methyl groups. It is possible, in principle, to determine these equilibrium configurations by microwave spectroscopy by studying the spectra of CH_2D species. That this has not been widely done is due to the expense and/or difficulty of preparing the isotopically-labelled compounds.

In spite of the uncertainty involved, two simple interpretations of the low barrier in N-methylformamide are especially attractive. In the first of these the low barrier is simply the result of cancellation of the nearly equal but opposite contributions to V_3 from the H_3CNH and H_3CNC fragments. That is, the methyl group faces two bonds 180^0 apart. Where these two bonds are equivalent, as in CH_3NO_2 (71), for example, it is known that $V_3 = 0$. In the present compound the non-equivalence of the NH and NC bonds leads to a net V_3 of 200 cal/mole. For this interpretation the NC amide bond would have to be an essentially single bond and the H····O steric effects must be ignored.

In the second simple interpretation the H_3CNH and H_3CNC fragments give rise to a relatively high V_3 contribution favoring an equilibrium configuration in which the methyl group staggers the NH bond. In this configuration

the H····O steric effect is most severe and increases the potential energy, thereby decreasing V_3. The net result is a V_3 of 200 cal/mole. For this interpretation the NC bond would have to be regarded as having significant double bond character and the H····O steric interaction must be significant. Which of these two interpretations is closer to the truth, if either, will have to be decided after further work.

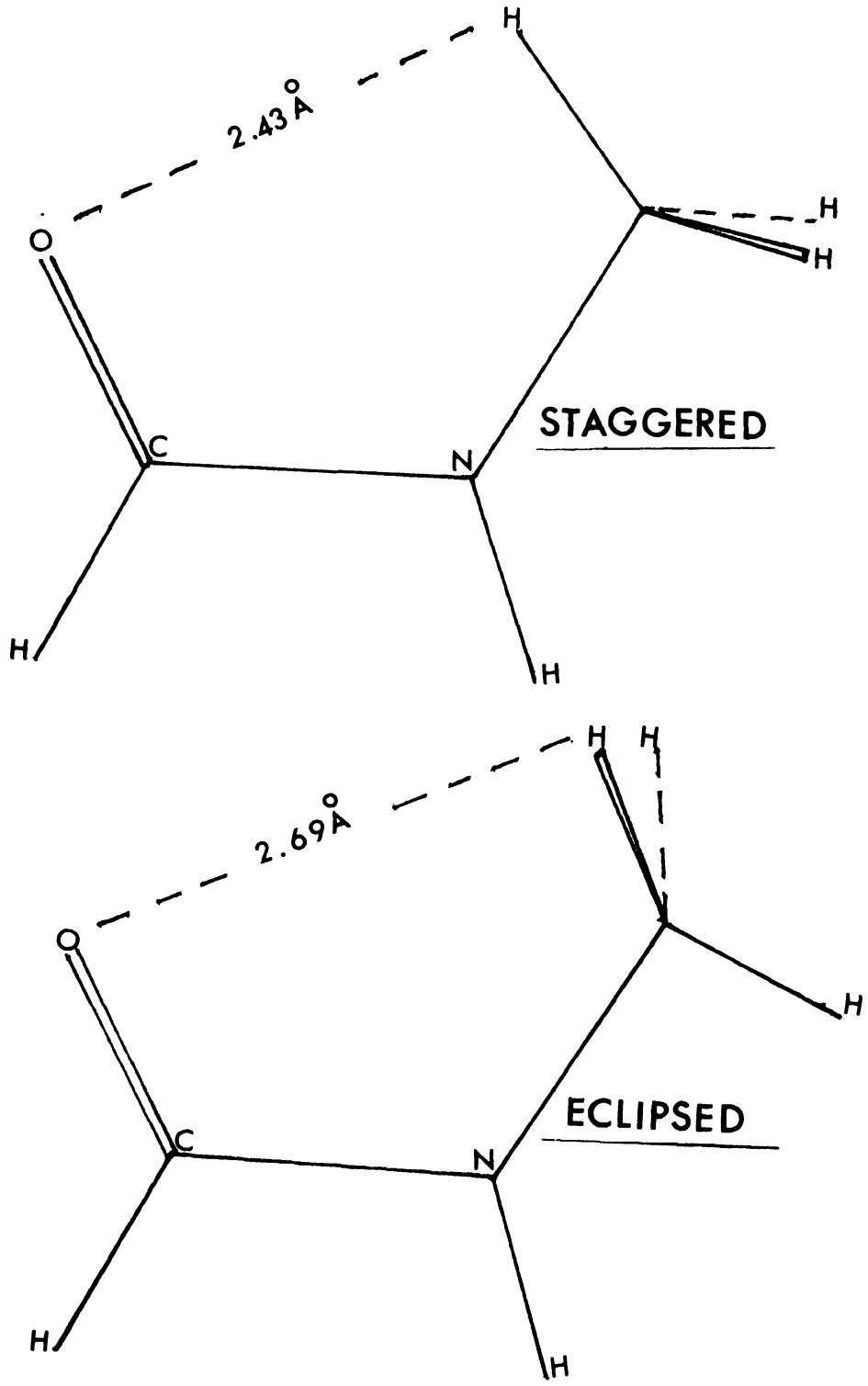

Figure V. Staggered and eclipsed conformations of cis N-methylformamide.

VI. DIMETHYLFORMAMIDE

6.1 Introduction

Dimethylformamide is a member of the class of compounds including the amides and polypeptides in which the N-C-O linkage has a major role in determining the structure and intramolecular dynamics. As mentioned before, Pauling (25) postulated that the central C-N bond in amides has an appreciable double-bond character. As a result of this double-bond character, amides and substituted amides should have planar or nearly planar skeletons. An electron diffraction study of DMF in the gas phase (72) showed that the compound is nearly planar. NMR studies of amides in solution (62) have shown the possibility of geometric isomerization about the C-N bond and barriers to internal rotation about this bond have been reported for several amides. Dielectric constant measurements (73) in the vapor phase at 110^0 for N-methylformamide and N,N-dimethylformamide gave values of the dipole moment as 3.82 and 3.80 Debyes, respectively.

Dimethylformamide (DMF), Figure VI, has been a subject of interest in this laboratory for several years. In 1968, H. B. Thompson assigned the ground state rotational spectrum of DMF-d_7, and also made a preliminary assignment for the parent

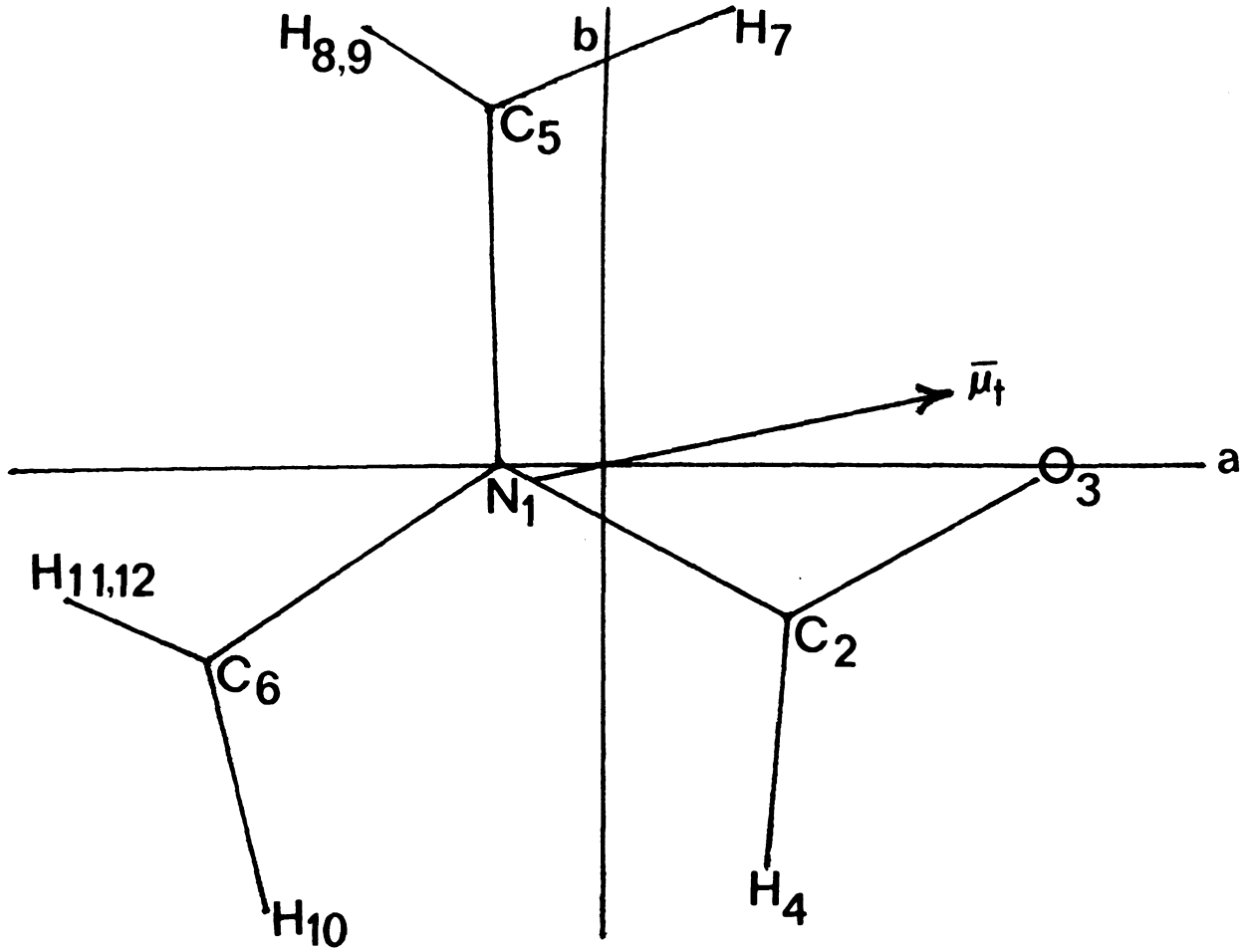

Figure VI. Projection of dimethylformamide onto the molecular symmetry plane. The probable orientation of the dipole moment vector, $\bar{\mu}_t$, is also shown.

compound. In 1969, A. H. Brittain restudied the rotational spectra for the two species and studied the Stark effects of several transitions.

In the present study the ground state rotational spectra of cis and trans DMF-d_3, Figure VII, were assigned. Rotational spectra in excited torsional states for both tops attached to the nitrogen atom were studied in all three isotopic species. The barrier to internal rotation of the methyl top cis to the oxygen atom was determined from the spectrum of trans DMF-d_3. The barrier was confirmed through the fitting of A and E-levels in the ground state rotational spectrum of the parent compound. Stark measurements were repeated and the dipole moment was determined for the parent compound.

6.2 Spectrum

The preliminary structural parameters of N,N-dimethylformamide were transferred from formamide (27). The rotational constants were calculated with the STRUCT computer program. The molecular parameters, atomic coordinates, and moments of inertia for the parent species are given in Tables 23 and 24. The moments of inertia for the other three isotopic species are also presented in Table 23. The inertial plane of symmetry for the compound is the a-b plane; therefore, a and b-type transitions should be observed. The preliminary rotational constants were used to calculate energy levels and transition frequencies.

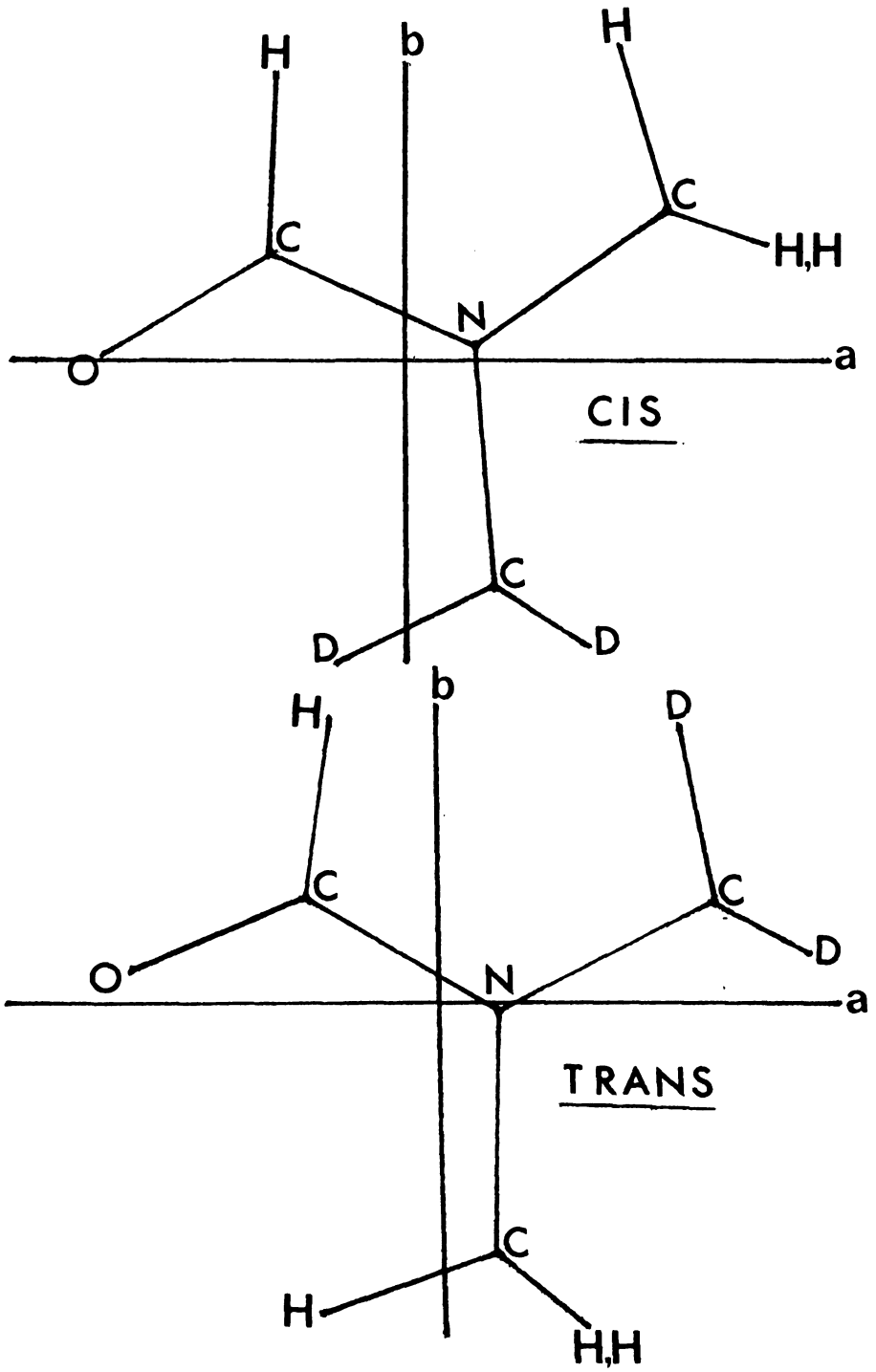

Figure VII. Projections of DMF-d_3 cis and trans onto their symmetry planes.

Table 23. Assumed structural and rotational parameters of DMF and its isotopic species.

Bond Distances and Bond Angles			
N_1C_2	1.376 Å	$N_1C_2O_3$	124.0°
N_1C_5	1.470	$O_3C_2H_4$	123.0°
C_2O	1.196	$N_1C_2H_4$	113.0°
C_2H_4	1.093	$C_2N_1C_5$	120.0°
C_5H_7	1.093	$N_1C_5H_7$	109.50°
N_1C_6	1.470	$H_{10}C_6H_{12}$	109.44°

Rotational Parameters[a]				
	DMF	cis DMF-d_3	trans DMF-d_3	DMF-d_7
I_a	58.7263	70.1023	64.0689	79.3343
I_b	119.1094	123.1452	132.9158	136.9717
I_c	171.4167	183.5003	187.2375	203.3131
κ	-0.5422	-0.3940	-0.5748	-0.3801

[a]Moments of inertia are in u.Å^2.

Table 24. Cartesian coordinates of the atoms of DMF in the principal axis system.[a]

Atom	a	b	c
N_1	-0.43198	-0.00158	0.0000
C_2	0.78462	-0.64442	0.0000
O_3	1.83917	-0.08019	0.0000
H_4	0.69219	-1.73350	0.0000
C_5	-0.48710	1.46737	0.0000
C_6	-1.67658	-0.78380	0.0000
H_7	0.52880	1.87060	0.0000
H_8	-1.01557	1.81265	0.89227
H_9	-1.01557	1.81265	-0.89227
H_{10}	-1.43724	-1.85027	0.0000
H_{11}	-2.25961	-0.54178	-0.89227
H_{12}	-2.25961	-0.54178	0.89227

[a]The coordinates shown here were calculated from the assumed structural parameters given in Table 23. The coordinates are in Å.

These calculations were performed by the EIGVALS computer program.

An initial search in the predicted spectral region revealed that each ground state rotational transition is accompanied at higher frequencies by several transitions of moderate intensity which exhibit a Stark effect identical to that of the main transition, as expected for vibrationally excited states. In this study confirmed assignments of the ground state rotational transitions for all isotopic species are presented here, while proposed assignments for the excited states are given in Appendix I. The reasons for this separation are discussed below.

A) Ground State Spectrum:

Although EIGVALS calculations indicated that each spectrume should consist of a- and b-type transitions, only a-type R-branch transitions were observed for all isotopic species. The assignments were substantiated by rigid-rotor fits and characteristic Stark effects. No splittings due to nitrogen quadrupole were observed, but on the other hand, measurable ground state splittings due to internal rotation were observed in both the parent and in the trans DMF-d_3 species.

Both A and E-level transitions were observed in most of the ground state transitions of trans DMF-d_3 and were confirmed through rigid-rotor fitting and theoretical calculation of the splittings. A comparison of observed and

calculated frequencies for a number of transitions is given in Table 25. After the barrier was determined for the methyl top, A and E-level transitions for the normal species were confirmed in a similar manner. A comparison of the observed and calculated frequencies for a number of transitions is given in Table 26.

As mentioned above, the ground state rotational transitions do not split in either the DMF-d_7 or the cis DMF-d_3 species. The absence of internal rotation splittings in the cis DMF-d_3 ground state transitions predicts a barrier for the methyl group trans to the aldehydic oxygen greater than 2000 cal/mole. A comparison of the observed and calculated frequencies for cis DMF-d_7, and DMF-d_7 are given in Tables 27 and 28, respectively. The ground state effective rotational parameters for all isotopic species are shown in Table 29.

B) Excited State Spectra:

Dimethylformamide and its isotopic species exhibit rich spectra in both the K and R-band spectral regions. Each ground state rotational transition is accompanied at higher frequencies by several transitions. These transitions are probably the corresponding rotational transitions in low-lying excited states of the methyl torsional motions. It was noticed that these excited states for cis DMF-d_3 occur more often in a consistent pattern. In this species each ground state transition is followed by three pairs of

Table 25. Observed rotational frequencies[a] and internal rotation splittings for <u>trans</u> DMF-d_3.

Transition	ν_A	ν_E	$(\nu_A - \nu_E)$
$3_{21} \rightarrow 4_{22}$	27281.45(0.04)[b]	27278.05(0.09)	3.40(-0.05)
$3_{12} \rightarrow 4_{13}$	27662.50(0.20)	27659.50(0.12)	3.0 (0.08)
$4_{14} \rightarrow 5_{15}$	29201.10(-0.03)	19201.10(0.64)	
$4_{23} \rightarrow 5_{24}$	32052.20(0.11)	32049.85(0.09)	2.35(-0.01)
$4_{32} \rightarrow 5_{33}$	32846.70(-0.08)	32843.60(-0.07)	3.10(0.00)
$4_{31} \rightarrow 5_{32}$	33183.85(-0.06)	33180.10(-0.19)	3.75(0.03)
$4_{13} \rightarrow 5_{14}$	34148.16(-0.14)	34145.02(-0.14)	3.14(0.04)
$4_{22} \rightarrow 5_{23}$	34589.10(0.05)	34584.61(0.06)	4.49(0.01)
$5_{15} \rightarrow 6_{16}$	34784.70(0.05)	34783.95(0.35)	0.75(-0.04)
$5_{05} \rightarrow 6_{06}$	35202.48(0.10)	35202.48(0.50)	
$5_{24} \rightarrow 6_{25}$	38166.38(-0.13)	38164.08(0.05)	2.30(-0.2)

[a] In MHz; estimated uncertainty is ±0.05 MHz.

[b] Values in parentheses are observed minus calculated frequencies. Rotational constants are in Table 29, internal rotation parameters in Table 30.

Table 26. Observed rotational frequencies[a] and internal rotation splittings for DMF.

Transition	ν_A	ν_E	$(\nu_A - \nu_E)$
$2_{02} \rightarrow 3_{03}$	20690.70(0.04)[b]	20689.50(0.12)	1.2 (-0.04)
$2_{20} \rightarrow 3_{21}$	22320.10(0.09)	22317.15(-0.2)	2.95(-0.15)
$2_{11} \rightarrow 3_{12}$	23217.10(0.08)	23214.30(0.19)	2.80(-0.2)
$3_{13} \rightarrow 4_{14}$	25830.00(0.03)	25829.10(0.00)	0.90(-0.1)
$3_{12} \rightarrow 4_{13}$	30648.90(-0.03)	30645.20(-0.12)	3.70(-0.02)
$4_{23} \rightarrow 5_{24}$	35369.20(-0.08)	35366.20(-0.21)	3.00(-0.03)
$4_{14} \rightarrow 5_{15}$	32019.90(-0.04)	32019.05(0.00)	0.95(-0.08)
$3_{21} \rightarrow 4_{22}$	30341.80(0.06)	30337.20(-0.10)	4.60(0.04)
$3_{22} \rightarrow 4_{23}$	28506.65(0.05)	28504.0(-0.1)	2.65(0.00)
$3_{31} \rightarrow 4_{32}$	39039.30(-0.07)	39036.55(0.1)	2.75(-0.05)

[a] In MHz; estimated uncertainty is ±0.05 MHz.

[b] Values in parentheses are observed minus calculated frequencies. Rotational constants are in Table 29; internal rotation parameters in Table 30.

Table 27. Comparison of observed and calculated frequencies[a] for cis DMF-d_3.

Transition	ν_{obs}	ν_{calc}	$\Delta\nu$[b]
$3_{30} \rightarrow 4_{31}$	28084.42	28084.59	-0.17
$3_{12} \rightarrow 4_{13}$	29164.27	29164.19	0.07
$3_{21} \rightarrow 4_{22}$	29444.35	29444.13	0.21
$4_{14} \rightarrow 5_{15}$	30008.67	30008.45	0.21
$4_{04} \rightarrow 5_{05}$	30409.54	30409.39	0.15
$4_{23} \rightarrow 5_{24}$	33505.22	33505.22	0.00
$4_{13} \rightarrow 5_{14}$	35617.40	35617.52	-0.12
$4_{31} \rightarrow 5_{32}$	35654.20	35654.66	-0.46
$5_{15} \rightarrow 6_{16}$	35656.76	35656.75	0.00
$5_{05} \rightarrow 6_{06}$	35848.40	35848.27	0.12
$4_{22} \rightarrow 5_{23}$	37221.82	37221.20	0.61
$5_{24} \rightarrow 6_{25}$	39700.11	39700.63	-0.52

[a] In MHz; estimated uncertainty in observed frequencies is ±0.05 MHz.

[b] $\nu_{obs} - \nu_{calc} = \Delta\nu$. Rotational constants are in Table 29.

Table 28. Comparison of observed and calculated frequencies[a] for DMF-d_7.

Transition	ν_{obs}	ν_{calc}	$\Delta\nu$[b]
$1_{01} \rightarrow 2_{02}$	12042.50	12042.41	0.08
$1_{10} \rightarrow 2_{11}$	13475.50	13475.38	0.11
$1_{11} \rightarrow 2_{12}$	11166.00	11165.93	0.06
$2_{11} \rightarrow 3_{12}$	20012.45	20012.53	-0.08
$2_{20} \rightarrow 3_{21}$	19501.70	19501.75	-0.05
$2_{21} \rightarrow 3_{22}$	18481.15	18480.99	0.15
$3_{13} \rightarrow 4_{14}$	21881.60	21881.66	-0.06
$3_{22} \rightarrow 4_{23}$	24421.60	24421.78	-0.18

[a] In MHz; estimated uncertainty in observed frequencies is ±0.05 MHz.

[b] $\nu_{obs} - \nu_{calc} = \Delta\nu$. Rotational constants are in Table 29.

Table 29. Ground state rotational parameters[a] for DMF and its isotopic species.

Parameter	DMF	trans DMF-d_3	cis DMF-d_3	DMF-d_7
A(MHz)	8927.80	8185.47	7494.36	6604.66
B	4203.77	3770.91	4061.47	3657.52
C	2964.67	2714.03	2772.34	2502.80
ΔA	1.91	0.51		
ΔB	0.69	0.57		
ΔC	-0.03	-0.02		
I_a(u.Å^2)	56.6069	61.7406	67.4341	76.5414
I_b	120.2196	134.0195	124.4317	138.2165
I_c	170.4661	186.2085	182.2919	201.9859
P_{aa}(u.Å^2)	117.0393	129.2437	119.6447	131.8305
P_{bb}	53.4267	56.9648	62.6471	70.1554
P_{cc}	3.1802	4.7757	4.7869	6.3860
κ	-0.5844	-0.6136	-0.4539	-0.4369

[a]Estimated uncertainty in rotational constants is ±0.7 MHz for A and ±0.04 MHz for B and C; $\Delta A = A_A - A_E$, etc.

doublets which have almost the same magnitude of splitting. One pair of these is relatively more intense than the other two, and seemed to be the first excited torsional state for the CD_3 top which has a barrier of 1079 cal/mole. The assumed A and E-level transitions fit the rigid-rotor model and the observed splittings agree nicely with the calculated splittings obtained by the INROT computer program. One of the other two pairs also fits the rigid rotor model and the comparison between the observed and calculated frequencies for this spectrum is given in Appendix I. The origin of this second set of doublets is not clear. It cannot be the second excited state of the CD_3 torsion because the splittings are too small. It cannot be the first excited of the CH_3 torsion because the splittings are too large. It cannot be a mixed mode because there is no more intense set of transitions to be the first excited state of the other mode.

A search for excited states in the normal and DMF-d_7 species disclosed a group of transitions to higher frequencies of the ground state lines. Among some of these transitions a similar pattern of doublets was observed which fit the rigid-rotor model as shown in Appendix I. The interpretation of these transitions is unclear.

The complexity of the spectra and the incoherence of the excited state transitions with respect to the ground state rotational transitions suggests the possibility of considerable coupling between the two tops attached to the

nitrogen atom. Preliminary calculations of the predicted spectra for two tops with coupled internal rotation with a computer program written by Dr. R. H. Schwendeman showed that the complexity of this problem is such as to be beyond the scope of this thesis.

6.3 Barrier to Internal Rotation

The analysis of internal rotation splittings in the ground state rotational transitions of DMF was carried out by using the effective Hamiltonian for each torsional state

$$H_{v\sigma} = H_r + F \sum_{n=1}^{4} W_{v\sigma}^{(n)} \rho^{(n)} \qquad (2\text{-}28)$$

The matrix elements of $H_{v\sigma}$ were calculated from Eq. (2-28) including perturbation coefficients to fourth order.

As mentioned above, the internal rotation splittings were observed in both DMF and DMF-d_3 (*trans*) in which the CH_3 top is *cis* to the carbonyl oxygen. The splittings were calculated by means of the INROT computer program. Assuming that $V_3 >> V_6$, only I_α, λ_g, A, B, C, and V_3 are variable parameters. Of these, the effective rotational constants were used from the assigned spectrum and the direction cosine, λ_g, was calculated from the assumed structure. The moment of inertia of the methyl top, I_α, was taken as 3.16 u.Å^2. The remaining adjustable parameter is V_3, the three-fold barrier to internal rotation. The difference between the observed and calculated splittings for *trans* DMF-d_3, and DMF normal species are given in Tables 25

and 26, respectively. The best value of V_3 is 1079 ± 10 cal/mole for trans DMF-d_3, and 1072 ± 10 cal/mole for normal DMF. These values are for the methyl group cis to the oxygen atom. All internal rotation parameters used in these calculations are given in Table 30.

6.4 Dipole Moment

It has been mentioned that the Stark effects provided an essential part of the evidence for assignment of DMF transitions. Most of these transitions exhibit clean and resolvable Stark components. The observed second-order Stark displacements in the frequencies of six Stark components were measured as a function of electric field (E). The Stark cell was calibrated by measuring the Stark shifts in the $J = 1 \rightarrow 2$ transition of OCS ($\mu_{OCS} = 0.7152$D (51)). The resulting six slopes, $d\Delta\nu/dE^2$, were used with Eq. (2-21) to calculate the dipole moment components, μ_a and μ_b ($\mu_c = 0$ if a plane of symmetry is assumed). The slopes were also fit by least-squares and the observed and calculated values along with the resulting value of the dipole moment are given in Table 31. For DMF $|\mu_a| = 3.795$ D, $|\mu_b| = 0.625$ D and $|\mu_t| = 3.845 \pm 0.02$ D; the angle between the dipole moment vector and the a axis is 9.35^0 and between the vector and CN internuclear line is 37.2^0. The latter value requires an assumption concerning the orientation of the dipole moment since only the squares of the components are obtained from the Stark effect. The

Table 30. Internal rotation parameters for the ground torsional states of DMF and DMF-d_3 (trans).

	DMF	DMF-d_3 (trans)
	Assumed	
I_α	3.16 u,Å^2	3.16 u Å^2
θ	87.81^0	88.08^0
λ_α	0.9992	0.9994
F	164.30265 GHz	163.84457 GHz
	Determined	
A_0	8926.57 MHz	8184.47 MHz
B_0	4203.76	3770.90
C_0	2964.67	2714.03
S	30.4134	30.6976
V_3	1072 ± 10 cal/mole	1079 ± 10 cal/mole

Table 31. Quadratic Stark coefficients and dipole moment of N,N-dimethylformamide.

Transition	|M|	$(\partial\nu/\partial E^2)_{obs}$ [a]	$(\partial\nu/\partial E^2)_{calc}$ [a]
$2_{12} \rightarrow 3_{13}$	0	-16.73	-16.10
	1	130.0	130.38
	2	568.70	569.71
$2_{11} \rightarrow 3_{12}$	0	-15.30	-14.67
	1	-110.66	-105.86
$2_{20} \rightarrow 3_{21}$	0	96.10	94.51

$|\mu_a| = 3.795 \pm 0.02$ D

$|\mu_b| = 0.625 \pm 0.01$ D

$|\mu_c| = 0.0$ D

$|\mu_t| = 3.845 \pm 0.02$ D

[a] In MHz/(Kvolt/cm)^2 assuming $\mu_{OCS} = 0.7152$ D.

orientation of the dipole moment assumed is that shown in Figure VI. Table 32 shows a comparison of reported dipole moments for several amides.

6.5 Discussion

There are three important results of the investigation of dimethylformamide and its isotopic species.

A) Planarity of DMF:

To test the planarity of the compound the effect of isotopic substitution on the inertial defect was applied in a manner similar to that proposed by Laurie (75). In this treatment expressions for the out-of-plane effective second moments of inertia for the parent and three other isotopic species (Table 29) are derived on the assumption of a plane of symmetry, as follows:

$$P_{cc}^{(p)} = \frac{I_\alpha^{(c)} + I_\alpha^{(t)}}{2} - \Delta/2$$

$$P_{cc}^{(c)} = \frac{I_\alpha^{(c)}\frac{m_D}{m_H} + I_\alpha^{(t)}}{2} - \Delta/2$$

$$P_{cc}^{(t)} = \frac{I_\alpha^{(t)}\frac{m_D}{m_H} + I_\alpha^{(c)}}{2} - \Delta/2$$

$$P_{cc}^{(d_7)} = \left(\frac{I_\alpha^{(c)} + I_\alpha^{(t)}}{}\right)\frac{m_D}{m_H} - \Delta/2$$

where $I_\alpha^{(c)}$ and $I_\alpha^{(t)}$ are the moments of inertia of the

Table 32. Comparison of dipole moments of some related amides.

Compound	μ_t[a]	Method[b]	Reference
Formamide	3.71	M.W.	74
N-methylformamide	3.856	M.W.	This Work
N,N-dimethylformamide	3.845	M.W.	This Work
Acetamide	3.75	D.C.	73
N-methylacetamide	3.71	D.C.	73
N,N-dimethylacetamide	3.80	D.C.	73
N-methylpropionamide	3.59	D.C.	73

[a]The total dipole moment in Debyes.

[b]M.W. indicates microwave spectroscopy; D.C. indicates dielectric constant measurements in the gas phase.

CH_3 tops cis and trans to the oxygen, respectively. The superscripts p, c, t, and d_7 on P_{cc} refer to parent, cis CD_3, trans CD_3 and d_7 species, respectively. From the first three values of P_{cc} it is found that Δ = 0.0538 u.Å^2 whereas Δ = 0.0466 u.Å^2 from the last three values. This is exceptional agreement for this kind of calculation and together with the reasonableness of the numbers suggests that the molecule has a plane of symmetry or nearly so. The difference in the Δ's could be the result of one or more of the following effects: 1) The I_α's are not the same in CD_3 tops as in CH_3 tops. 2) The Δ's are not the same in all species. 3) DMF-d_7 contains a deuterium in the CHO part, 4) The A rotational constants needed to calculate the P_{cc}'s are not as precise as desired (± 1 MHz).

B) Barrier to Internal Rotation:

One result of the present study of dimethylformamide is that for the methyl group cis to the oxygen atom the barrier to internal rotation (V_3 = 1079 cal/mole) is approximately 900 cal/mole higher than the corresponding barrier height in cis N-methylformamide (V_3 = 200 cal/mole). In the discussion above of the barrier in N-methylformamide two simple interpretations were given for the rather low barrier height in that compound. Since neither of the interpretations would be expected to be altered in DMF, the higher barrier in this compound is most easily explained as

being the result of an interaction between the two methyl groups, perhaps a gearing effect. As pointed out above, there are evidences in the spectra of the excited torsional states of some of the species that a top-top interaction is taking place and that further analysis of this effect is in progress. It should be pointed out, however, that the microwave spectrum of dimethylamine has been interpreted without considering top-top interaction terms. Also, the higher barrier in DMF compared to N-methylformamide matches a corresponding trend in methylamine (V_3 = 1976 cal/mole (67)), dimethylamine (V_3 = 3200 cal/mole (70)), and trimethylamine (V_3 = 4400 cal/mole (76)).

The relatively high barrier to internal rotation (V_3 > 2 kcal/mole) for the methyl group trans to the oxygen atom in DMF may be interpreted as favoring the steric mechanism involving an O····H interaction for the low barrier in N-methylformamide. This is because the contributions from the H_3CNH and H_3CNC fragments should be comparable for both methyl groups in DMF. The O····H interaction is absent for the methyl group trans to oxygen, however. It is replaced by an H····H interaction in which the two hydrogen atoms never approach distances which are smaller than the sum of the van der Waals' radii.

It should be reemphasized here that these are highly speculative and tentative interpretations. Much more work on internal rotation in methyl groups attached to nitrogen is needed.

C) Dipole Moment:

The dipole moment obtained for DMF is slightly smaller than that of N-methylformamide, and both have values of dipole moment slightly greater than the corresponding values obtained from dielectric constant measurements (NMF 3.82 D (73); DMF 3.80 D (73)). It is apparent from the comparison in Table 33 that the amide group itself can be assigned a moment of 3.75 D, with the variation in the dipole moment due to various alkyl groups having a net effect of only ±0.15D.

REFERENCES

REFERENCES

(1) C. H. Townes and A. L. Schawlow, Microwave Spectroscopy (McGraw-Hill, N.Y., 1955).

(2) J. E. Wollrab, Rotational Spectra and Molecular Structure (Academic Press, N.Y., 1967).

(3) W. Gordy, W. V. Smith, R. F. Trambarulo, Microwave Spectroscopy (Wiley, N.Y., 1953).

(4) M. W. P. Strandberg, Microwave Spectroscopy (Methuen, London, 1954).

(5) T. M. Sugden and C. N. Kenny, Microwave Spectroscopy of Gases (Van Nostrand, Princeton, N.J., 1965).

(6) C. E. Cleeton and N. H. Williams, Phys. Rev. 45, 234 (1934).

(7) D. O. Harris, G. G. Engerholm, C. A. Tolman, A. C. Luntz, R. A. Keller, H. Kim, and W. D. Gwinn, J. Chem. Phys. 50, 2438 (1969).

(8) L. H. Scharpen, J. S. Muenter, and V. W. Laurie, J. Chem. Phys. 46, 2437 (1967).

(9) W. H. Flygare and R. C. Benson, Mol. Phys. 20, 225-250 (1971).

(10) T. Oka, J. Chem. Phys. 49, 3135 (1968).

(11) E. B. Wilson, Jr., Science, 162, 59 (1968).

(12) H. Goldstein, Classical Mechanics,(Addison-Wesley Publishing Company, Inc., Reading, Mass., 1950) p. 149.

(13) J. L. Synge, B. A. Griffith, Principles of Mechanics, Second Edition, (McGraw-Hill Book Company, Inc., N.Y. 1949) p. 313.

(14) R. H. Schwendeman, J. Mol. Spectr. 6, 301 (1961).

(15) G. W. King, R. M. Hainer, and P. C. Cross, J. Chem. Phys. 11, 27 (1943).

(16) J. H. Van Vleck, Phys. Rev. 33, 467 (1929).

(17) B. S. Ray, Zeits. f. Physik 78, 74 (1932).

(18) D. M. Dennison, Rev. Mod. Phys. 3, 280 (1931).

(19) P. C. Cross, R. M. Hainer, G. W. King, J. Chem. Phys. 12, 120 (1944).

(20) S. Golden and E. B. Wilson, Jr., J. Chem. Phys. 16, 669 (1948).

(21) Lin, C. C., and J. D. Swalen, Rev. Mod. Phys. 31, 841 (1959)

(22) D. R. Herschbach, J. Chem. Phys. 31, 91 (1959).

(23) H. H. Nielsen, Phys. Rev. 40, 445 (1932).

(24) J. S. Koehler and D. M. Dennison, Phys. Rev. 57, 1006 (1940).

(25) L. Pauling, The Nature of Chemical Bond (Univ. Press, Ithaca, 1948).

(26) R. J. Kurland, J. Chem. Phys. 23, 2202 (1955).

(27) C. C. Costain and J. M. Dowling, J. Chem. Phys. 32, 158 (1960).

(28) J. K. Tyler, L. F. Thomas, and J. Sheridan, Proc. Chem. Soc. P., 155 (1959).

(29) D. J. Millen, G. Topping, and D. R. Lide, J. Mol. Spectr. 8, 153 (1962).

(30) T. Oka, Y. Morino, J. Mol. Spectr. 6, 472 (1961).

(31) T. Oka, Y. Morino, J. Mol. Spectr. 8, 9 (1962).

(32) H. H. Nielsen, Revs. Mod. Phys. 23, 90 (1951).

(33) G. Heitzberg, Infrared and Ramman Spectra, (VanNostrand, New York, 1945) p. 220.

(34) M. F. Manning, J. Chem. Phys. 3, 136 (1935).

(35) J. Kraitchman, Am. J. Phys. 21, 17 (1953).

(36) V. Kumar and A.S.N. Murty, Indian J. Pure Appl. Phys. 7, 597 (1969).

(37) R. H. Hughes and E. B. Wilson, Jr., Phys. Rev. 71, 562 (1947).

(38) A. H. Sharbaugh, Rev. Sci. Instr. 21, 120-135 (1950).

(39) A. H. Brittain, J. E. Smith, and R. H. Schwendeman, Inorg. Chem., 11, 39 (1972).

(40) A. H. Brittain, J. E. Smith, P. L. Lee, K. Cohn, and R. H. Schwendeman, J. Amer. Chem. Soc. 93, 6772 (1971).

(41) P. L. Lee, K. Cohn, and R. H. Schwendeman, Inorg. Chem. 11, 1917 (1972).

(42) E. G. Codding, Ph.D. Thesis, Michigan State University, 1971, Sections 5, 6.

(43) R. L. Kuczkowski, J. Am. Chem. Soc. 90, 1705 (1968).

(44) P. S. Bryan and R. L. Kuczkowski, Inorg. Chem. 11, 553 (1972).

(45) J. P. Paniski and R. L. Kuczkowski, J. Chem. Phys. 54, 1903 (1971).

(46) R. L. Kuczkowski and D. R. Lide, Jr., J. Chem. Phys. 46, 357 (1967).

(47) R. L. Foester and K. Cohn, Inorg. Chem., In Press.

(48) J. H. Hand, Ph.D. Thesis, Michigan State University, 1965.

(49) R. H. Schwendeman, J. Mol. Spectr. 7, 280 (1961).

(50) H. N. Voltrauer, Ph.D. Thesis, Michigan State University, 1970, Section 4.

(51) J. S. Muenter, J. Chem. Phys. 48, 4544 (1968).

(52) R. J. Gillespie, J. Chem. Ed. 47, 18 (1970).

(53) H. A. Bent, J. Inorg. Nucl. Chem. 19, 43 (1961).

(54) D. W. J. Cruickshank, J. Chem. Soc., 5486 (1961).

(55) K. F. Purcell, Inorg. Chem. 11, 891 (1972).

(56) I. M. Mills, Spectrochim. Acta 19, 1585 (1963).

(57) W. D. Phillips, J. Chem. Phys. 23, 1363 (1955).

(58) S. Mizushima, Structure of Molecules (Academic Press, Inc., New York, 1954) pp. 117-152.

(59) W. E. Kellner, J. Chem. Phys. 16, 1003 (1948) and R. D. Waldron and R. M. Badger, J. Chem. Phys. 18, 566 (1950).

(60) J. Zabicky, Ed., The Chemistry of Amides (Interscience, New York, 1970).

(61) L. A. LaPlanche and M. T. Rogers, J. Amer. Chem. Soc., 86, 337 (1964).

(62) L. R. Isbrandt, Ph.D. Thesis, Michigan State University, 1972, page 93.

(63) R. A. Russell, and H. W. Thompson, Spectr. Acta 8, 138 (1956).

(64) D. R. Herschbach and V. W. Laurie, J. Chem. Phys. 40, 3142 (1964).

(65) R. S. Rogowski, Ph.D. Thesis, Michigan State University, 1968, Section 6.

(66) H. D. Rudolph, Z. Naturforsch. 23a, 540 (1968).

(67) T. Itoh, J. Phys. Soc. Japan 11, 264 (1956).

(68) K. V. L. N. Sastry and R. F. Curl, Jr., J. Chem. Phys. 41, 77 (1964).

(69) J. Meier, A. Bauder, and Hs. H. Gunthard, J. Chem. Phys. 57, 1219 (1972).

(70) V. W. Laurie and J. Wollrab, Bull. Am. Phys. Soc., Ser. II8, 327 (1963).

(71) E. Tannenbaum, R. J. Myers, and W. D. Gwinn, J. Chem. Phys. 25, 42 (1956).

(72) L. V. Vilkov, P. A. Akishin, and V. M. Presnyakova, Zh. Strukt. Khim. 3, 5-9 (1962).

(73) R. M. Meighan and R. H. Cole, J. Phys. Chem. 68, 503 (1964).

(74) R. J. Kurland and E. B. Wilson, Jr., J. Chem. Phys. 27, 585 (1964).

(75) V. W. Laurie, J. Chem. Phys. 28, 704 (1958).

(76) D. R. Lide, Jr., and D. E. Mann, J. Chem. Phys. 28, 572 (1958).

APPENDIX I

APPENDIX I

The following tables of frequencies of rotational transitions in DMF and its isotopic species are given probable assignments as the low-lying first excited states for the CH_3 and CD_3 torsional motions.

Table 33. Frequencies[a] of A-level transitions for the $v = 1$ torsional motion of CH_3 (trans to the oxygen) of DMF.

Transition	ν_{obs}	$\Delta\nu$[b]
$3_{03} \rightarrow 4_{04}$	26895.0	0.03
$3_{22} \rightarrow 4_{23}$	28559.30	0.10
$3_{12} \rightarrow 4_{13}$	30694.20	0.11
$4_{23} \rightarrow 5_{24}$	35435.8	-0.07
$4_{31} \rightarrow 5_{32}$	36886.20	-0.02
$4_{13} \rightarrow 5_{14}$	37813.30	-0.08

[a] In MHz.

[b] $\Delta\nu = \nu_{obs} - \nu_{calc}$; the calculated frequencies are obtained from the rotational constants given in Table 38

Table 34. Frequencies[a] of A and E-level transitions for the v = 1 torsional motion of the CH_3 group of cis DMF-d_3.

Transition	ν_A	ν_E
$3_{22} \rightarrow 4_{23}$	27131.80(0.07)[b]	27136.30(0.40)
$3_{31} \rightarrow 4_{32}$	27864.30(1.74)	27869.10(1.16)
$4_{14} \rightarrow 5_{15}$	30042.90(-0.07)	30044.50(0.3)
$4_{04} \rightarrow 5_{05}$	30438.20(0.21)	30439.30(0.43)
$4_{23} \rightarrow 5_{24}$	33543.80(0.16)	33548.40(0.19)
$4_{32} \rightarrow 5_{33}$	34864.50(-1.20)	34871.08(-1.26)
$4_{22} \rightarrow 5_{23}$	37273.65(-0.19)	37283.20(0.08)
$5_{24} \rightarrow 6_{25}$	39743.08(-0.09)	39747.52(-0.31)
$5_{15} \rightarrow 6_{16}$	35697.10(-0.19)	35698.18(-0.18)

[a] In HMz.

[b] The quantities given in the parentheses are ($\nu_{obs} - \nu_{calc}$). The calculated frequencies are obtained from the rotational constants shown in Table 38.

Table 35. Frequencies[a] of A and E-level transitions for the v = 1 torsional motion of the CD_3 group of cis DMF-d_3.

Transition	ν_A	ν_E
$3_{22} \rightarrow 4_{23}$	27157.80(0.02)[b]	27162.40(0.32)
$3_{31} \rightarrow 4_{32}$	27888.50(0.00)	27895.0 (0.66)
$4_{04} \rightarrow 5_{05}$	30468.60(-0.22)	30469.40(0.09)
$4_{23} \rightarrow 5_{24}$	33576.10(-0.18)	33581.0 (0.14)
$4_{13} \rightarrow 5_{14}$	35684.80(0.50)	35688.90(0.04)
$4_{31} \rightarrow 5_{32}$	35744.90(0.13)	35754.40(-0.28)
$4_{22} \rightarrow 5_{23}$	37308.14(-0.09)	37318.09(-0.07)
$5_{24} \rightarrow 6_{25}$	39781.85(-0.55)	39786.24(-0.62)

[a] In MHz

[b] The values given in parentheses are ($\nu_{obs} - \nu_{calc}$). The calculated frequencies are obtained from the rotational constants given in Table 38.

Table 36. Frequencies[a] of A and E-level transitions for the v = 1 torsional motion of CD_3 (cis to the oxygen) of DMF-d_7.

Transition	ν_A	ν_E
$3_{21} \rightarrow 4_{22}$	26613.0 (-0.04)	26620.50(-0.18)
$4_{22} \rightarrow 5_{23}$	33613.0 (0.03)	33621.80(0.14)
$5_{15} \rightarrow 6_{16}$	32208.80(0.05)	32209.80(0.23)
$5_{05} \rightarrow 6_{06}$[c]	32361.50(-0.05)	32361.50(-0.23)
$6_{06} \rightarrow 7_{07}$[c]	37329.0 (-0.3)	37329.0 (-0.63)
$6_{16} \rightarrow 7_{17}$[c]	37264.8 (0.1)	37264.8 (-0.63)

[a] In MHz.

[b] The values given in parentheses are ($\nu_{obs} - \nu_{calc}$). The calculated frequencies are obtained from the rotational constants given in Table 38.

[c] Unresolved transitions.

Table 37. Frequencies[a] of A-level transitions for the v = 1 torsional motion of CD_3 (trans to the oxygen) of DMF-d_7.

Transition	ν_{obs}	$\Delta\nu$[b]
$4_{22} \rightarrow 5_{23}$	33586.50	0.00
$5_{05} \rightarrow 6_{06}$	32306.60	0.22
$5_{15} \rightarrow 6_{16}$	32154.80	0.06
$5_{24} \rightarrow 6_{25}$	35770.50	0.00
$6_{16} \rightarrow 7_{17}$	37201.00	-0.05
$6_{06} \rightarrow 7_{07}$	37265.0	0.00

[a] In MHz.

[b] $\Delta\nu = \nu_{obs} - \nu_{calc}$, the calculated frequencies are obtained from the rotational constants given in Table 38.

Table 38. Rotational parameters of the first excited torsional states for DMF and its isotopic species.

Parameter[a]	DMF	cis DMF-d_3		DMF-d_7	
		CH_3	CD_3	CD_3 (cis)	CD_3 (trans)
A_A (MHz)	8914.42	7473.71	7485.90	6597.62	6590.40
B_A	4208.16	4066.58	4070.43	3662.79	3660.61
C_A	2973.29	2775.99	2778.63	2508.15	2503.46
P_{aa} (u.Å^2)	116.6868	119.3535	119.2632	131.4345	131.6223
P_{bb}	53.2846	62.6988	62.6159	70.0588	70.2481
P_{cc}	3.4073	4.9215	4.8944	6.5408	6.4354
κ	-0.5842	-0.4505	-0.4511	-0.4353	-0.4337

[a]Estimated uncertainties in rotational constants are ±1.0 MHz for A , and ±0.04 MHz for B and C.